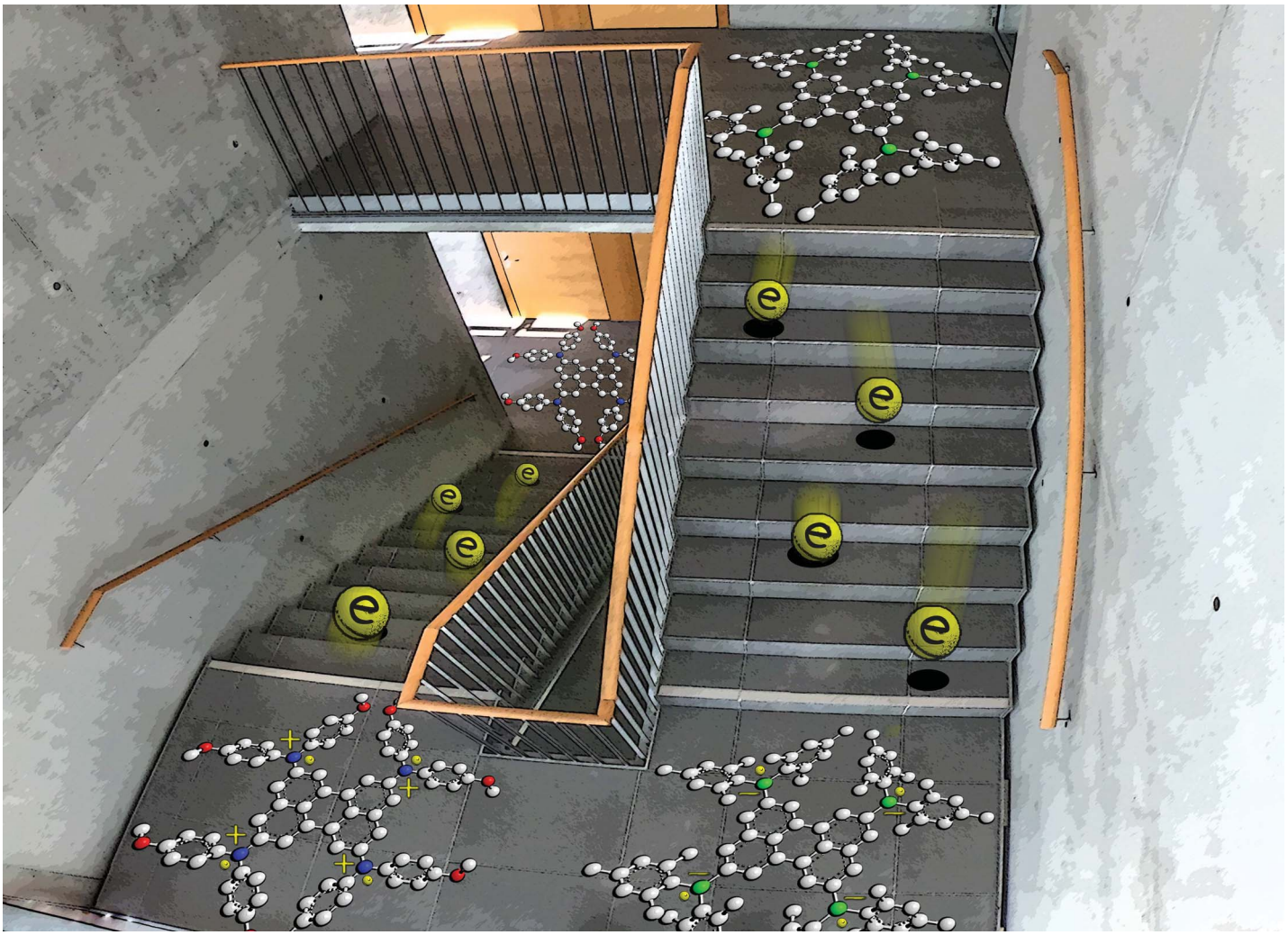

Showcasing research from Professor Marder's laboratory, Institut für Anorganische Chemie and Institute for Sustainable Chemistry & Catalysis with Boron (ICB), Julius-Maximilians-Universität Würzburg, Würzburg, Germany.

Synthesis, photophysical and electronic properties of tetra-donor- or acceptor-substituted *ortho*-perylenes displaying four reversible oxidations or reductions

The drawing by Dr. Stefanie Griesbeck depicts the work of Dr. Julia Merz, Prof. Dr. Christoph Lambert, Prof. Dr. Todd B. Marder and their co-workers on the synthesis of perylene derivatives containing either 4 donor or 4 acceptor groups located at the *ortho* positions. Detailed characterization of the optical and electronic properties of the resulting compounds includes absorption and emission spectroscopy, luminescent detection of singlet oxygen formation, transient absorption studies of the excited states, electrochemistry and spectroelectrochemistry, DFT and TD-DFT calculations, and single-crystal X-ray diffraction studies.

As featured in:

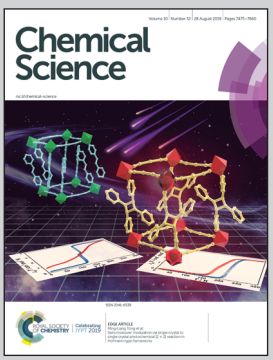

See Todd B. Marder *et al.*, *Chem. Sci.*, 2019, **10**, 7516.

ROYAL SOCIETY OF CHEMISTRY | Celebrating IYPT 2019

rsc.li/chemical-science

Registered charity number: 207890

Chemical Science

EDGE ARTICLE

View Article Online
View Journal | View Issue

Cite this: *Chem. Sci.*, 2019, **10**, 7516

All publication charges for this article have been paid for by the Royal Society of Chemistry

Synthesis, photophysical and electronic properties of tetra-donor- or acceptor-substituted *ortho*-perylenes displaying four reversible oxidations or reductions†

Julia Merz,[a] Andreas Steffen,[ab] Jörn Nitsch,[a] Julian Fink,[a] Claudia B. Schürger,[a] Alexandra Friedrich,[a] Ivo Krummenacher,[a] Holger Braunschweig,[a] Michael Moos,[c] David Mims,[c] Christoph Lambert[c] and Todd B. Marder[*a]

Via regioselective Ir-catalyzed C–H borylation and subsequent reactions (*i.e.*, *via* **Br_4-Per** or **$(BF_3K)_4$-Per** intermediates), we have introduced strong π-donors and acceptors at the 2,5,8,11-positions of perylene leading to unusual properties. Thus, incorporation of four donor diphenylamine (DPA) or four acceptor $Bmes_2$ (mes = 2,4,6-$Me_3C_6H_2$) moieties yields novel compounds which can be reversibly oxidized or reduced four times, respectively, an unprecedented behavior for monomeric perylene derivatives. Spectroelectrochemical measurements show NIR absorptions up to 3000 nm for the mono-cation radical of **$(DPA)_4$-Per** and a strong electronic coupling over the perylene bridge was observed indicative of fully delocalized Robin-Day Class III behavior. Both **$(DPA)_4$-Per** and **$(Bmes_2)_4$-Per** derivatives possess unusually long intrinsic singlet lifetimes (τ_0), *e.g.*, 94 ns for the former one. The compounds are emissive in solution, thin films, and the solid state, with apparent Stokes shifts that are exceptionally large for perylene derivatives. Transient absorption measurements on **$(DPA)_4$-Per** reveal an additional excited state, with a long lifetime of 500 μs, which sensitizes singlet oxygen effectively.

Received 17th May 2019
Accepted 20th June 2019

DOI: 10.1039/c9sc02420d

rsc.li/chemical-science

Introduction

Polycyclic aromatic hydrocarbons (PAHs) show very different and unusual properties compared to small aromatic compounds as a result of their extended π-conjugation. Their narrower HOMO–LUMO gaps lead to long-wavelength absorptions and emissions. Furthermore, PAHs such as perylene have lower oxidation and/or reduction potentials, higher mechanical strengths and stronger π–π-interactions.[1,2] Perylene diimides (PDIs) have attracted much interest for use as dyes, pigments[3,4] and semiconductors[5] in diverse applications.[6–12] They exhibit high chemical, thermal and photochemical stability, strong absorption and fluorescence and unique self-assembly behavior, which facilitates charge mobility.[13–18] In addition, their high electron affinity makes PDIs promising candidates for electronic materials such as organic field effect transistors and solar cells.[12,13,19,20]

The perylene core has 12 positions and can be considered as two naphthalene moieties conjoined at the 1 and 8 positions (Fig. 1).[21] Diamagnetic susceptibility studies indicate that the central ring of perylene fails to display fully aromatic character as the naphthalene units dominate the perylene structure.[21–23] Furthermore, Nucleus-Independent Chemical Shift (NICS) calculations indicate that the central ring is non-aromatic[24] and X-ray structural data demonstrates that the C–C bonds joining the two naphthalene units are relatively long compared to typical aromatic C–C bonds. For the β polymorph of perylene, a C6a–C6b (or C12a–C12b) bond length of 1.474(1) Å was reported at 130 K from single-crystal X-ray diffraction data,[25] while a bond length of 1.467(4) Å was reported at 200 K by Botoshansky *et al.*[26] For the α polymorph of perylene, C6a–C6b (or C12a–C12b) bond lengths were reported to be in the range of 1.462–1.480 Å.[26–28] These distances are typical of $C(sp^2)$–$C(sp^2)$ single bonds.[29–31]

This combination of two connected naphthalene units leads to particular photophysical properties. Substituting naphthalene at its 1 and 8 positions leads to a modulation of its L_a transition in such a way that in perylene the $S_1 \leftarrow S_0$ transition is polarized along the *z*-axis (L_a) and not along the *y*-axis (L_b) as in naphthalene. Perylene's lowest-lying singlet excited state,

[a]*Institut für Anorganische Chemie, Institute for Sustainable Chemistry & Catalysis with Boron (ICB), Julius-Maximilians-Universität Würzburg, Am Hubland, 97074 Würzburg, Germany. E-mail: todd.marder@uni-wuerzburg.de*

[b]*Faculty of Chemistry and Chemical Biology, TU Dortmund University, Otto-Hahn-Str. 6, 44227 Dortmund, Germany*

[c]*Institut für Organische Chemie, Julius-Maximilians-Universität Würzburg, Am Hubland, 97074 Würzburg, Germany*

† Electronic supplementary information (ESI) available. CCDC 1881912. For ESI and crystallographic data in CIF or other electronic format see DOI: 10.1039/c9sc02420d

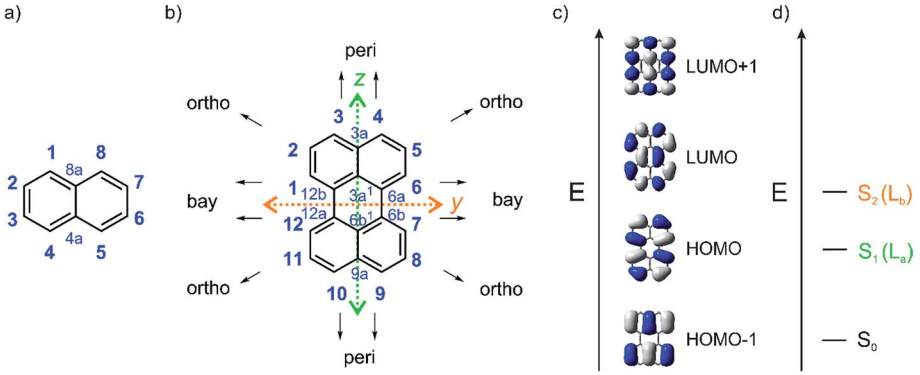

Fig. 1 (a) Atom numbering system in naphthalene; (b) atom numbering system with principle Cartesian coordinate system used for perylene; (c) the four frontier orbitals of perylene; and (d) low energy optical transitions of perylene with the Platt nomenclature.[32]

observed in the absorption spectrum at 440 nm (ε = 34 000 M^{-1} cm^{-1} in toluene), consists of four vibrational sub-bands with a 1400 cm^{-1} interval and is assigned to a symmetry allowed HOMO → LUMO transition.[33–35] The *y*-axis-polarized (L_b) S_2 ← S_0 transition at 253 nm (ε = 52 000 M^{-1} cm^{-1} in hexane) is energetically well separated from S_1 by 16 800 cm^{-1}. As the S_1 ← S_0 transition is allowed, emission from S_1 is also (λ_{max}(em) = 444 nm in toluene) allowed and, therefore, the intrinsic lifetime (τ_0) of 5.5 ns is quite short, and fluorescence is strong with a quantum yield near unity.[35] **PDI-A's** (Fig. 2) lowest energy *z*-axis-polarized (L_a) absorption is observed at 526 nm in chloroform, and is stronger than perylene's with ε = 88 000 M^{-1} cm^{-1}.[13,36] This compound emits in the yellow-green region at 533 nm in chloroform with τ_0 = 4 ns.

As perylenes play an important role in electronic materials, their electronic properties have been studied by several groups.[37,38] Cyclic voltammetry measurements show that unsubstituted perylene can be reversibly reduced to its radical anion at −2.07 V and dianion at −2.66 V *vs.* Fc/Fc^+ (DMF/MeCN) and reversibly oxidized at +0.69 V *vs.* Fc/Fc^+ (Table 1).[5,38,39] PDIs are a class of compounds that are very easy to reduce, with **PDI-A** having a reduction potential of −0.98 V *vs.* Fc/Fc^+. Further substitution can give rise to even stronger oxidants.[13]

However, perylene derivatives without carboxyimide groups at the *peri* positions are much less well studied due to difficulties in functionalizing the perylene core directly.[43–45] One method to functionalize perylene directly is *via* Ir-catalyzed C–H borylation, which was reported by Marder and co-workers in 2005.[45] As a result of the very crowded nature of the active five-

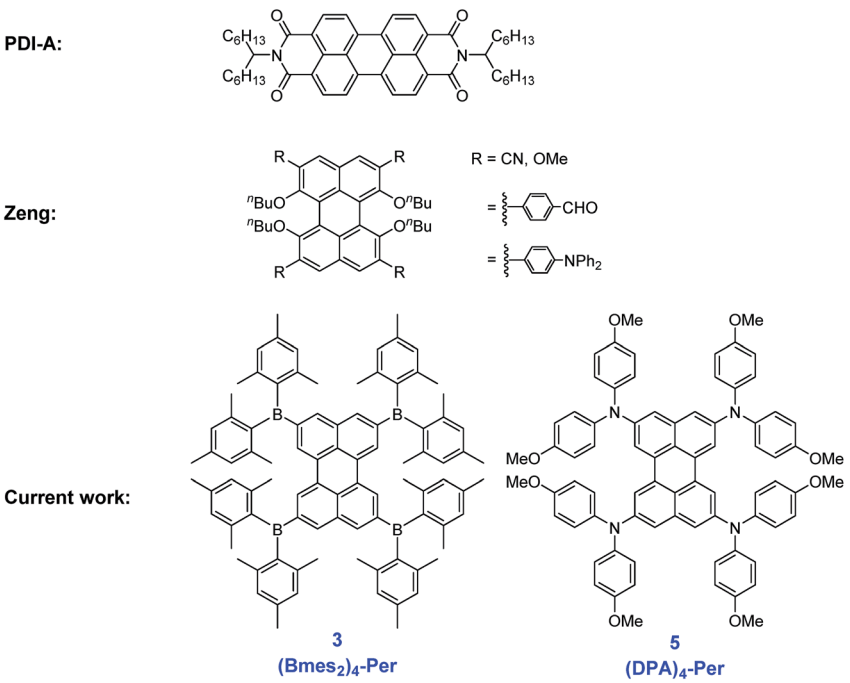

Fig. 2 Examples of known perylene derivatives[13,44] and our two target perylene derivatives.

Table 1 Redox properties of perylene and PDI

	$E_{1/2}$[red]^1	$E_{1/2}$[red]^2	$E_{1/2}$[ox]
Perylene	−2.07 V *vs.* Fc/Fc^+ (MeCN)[5,38,39]	−2.66 V *vs.* Fc/Fc^+ (DMF)[5,37]	+1.25 V *vs.* Fc/Fc^+ (MeCN)[5,38]
	−1.67 V *vs.* SCE (DMF/MeCN)[38,39]	−2.21 V *vs.* SCE (DMF)[37]	+1.09 V *vs.* NHE (DMF or MeCN)[38]
	−1.63 V *vs.* SCE (THF)[37]	−2.17 V *vs.* SCE (THF)[37]	+0.85 V *vs.* SCE (MeCN)[40,41]
PDI-A	−0.98 V *vs.* Fc/Fc^+ (MeCN)[42]	−1.21 V *vs.* Fc/Fc^+ (MeCN)[42]	+1.21 V *vs.* Fc/Fc^+ (MeCN)[42]
	−0.58 V *vs.* SCE[5]	−0.81 V *vs.* SCE[5]	+1.61 *vs.* SCE[5]

coordinate Ir(III)-catalyst, borylation of C–H bonds *ortho* to a substituent or ring junction is inhibited.[46] Therefore, it is possible to borylate the 2,5,8,11-positions of perylene selectively, providing a useful entry point for the synthesis of diverse *ortho* substituted perylene derivatives.[47,48] In 2011, Shinokubo and co-workers[49,50] employed a modified Ir-catalyzed borylation reaction with an *ortho* directing ligand, which enabled the functionalization of the four *ortho* positions of PDI's with heteroaryl, OMe and OH moieties for the first time. They observed a slight blue-shift in the absorption (from 525 to 512 nm) and emission (from 533 to 516 nm) spectra through the introduction of OH groups, which is caused by an intramolecular hydrogen bonding interaction between the carbonyl and hydroxy groups. The OMe moieties on the other hand, cause a small red shift in the absorption (from 525 to 538 nm) and emission (from 533 to 549 nm) spectra. In 2012, a Suzuki–Miyaura cross-coupling was reported by Ikeda *et al.* using 2,5,8,11-tetra(Bpin)perylene to give a porphyrin-perylene-porphyrin triad[51] and, in 2016, Tran *et al.* reported Suzuki–Miyaura coupling of our 2,5,8,11-tetra(Bpin)perylene to give microporous coordination polymers.[52] However, there are no reports so far of only *ortho* heteroatom substituted perylenes. Thus, investigations of the effect of substituents on the 2,5,8,11-positions of the perylene core are still lacking. In 2017, Zeng and co-workers[44] prepared *ortho* and *bay* octa-substituted perylene derivatives by an indirect method, namely oxidative radical–radical coupling of two naphthene units followed by reduction. They synthesized 2,5,8,11-tetrabromo-1,6,7,12-tetra-*n*-butoxyperylene and showed the versatility of that derivative by performing Suzuki–Miyaura coupling reactions and nucleophilic substitution reactions with copper cyanide or sodium methoxide to place cyano or methoxy moieties at the *ortho* positions. However, the *n*-butoxy substituents at the *bay* positions lead to a twisted core, which influences the properties of these perylene derivatives. In 2017, Hariharan, Shaijumon and co-workers demonstrated, with a twisted PDI, that the energy levels of the reduced species are altered and a single plateau discharge profile can be achieved, which is crucial for rechargeable battery electrodes.[53] To investigate the influence of substitution only at the *ortho* positions on the perylene core, we prepared an *ortho* perylene derivative with four donors (D) and one with four acceptors (A), due to their strong influence on the frontier orbital levels.

Materials with high HOMO energies, such as the compound *N*,*N*′-diphenyl-*N*,*N*′-bis(3-methylphenyl)-(1,1′-biphenyl)-4,4′-diamine (TPD), are especially useful for hole transport.[54–60] Common π-donors that have been used in dyes to boost HOMO energies include amines, with a lone pair on the nitrogen, such as diarylamino, diethylamino, dimethylamino or carbazolyl moieties.[61] Diarylamines are among the strongest π-electron donors and have been employed in diverse applications,[62–74] due to their outstanding physical, photochemical and electrochemical properties. Furthermore, they are easy to synthesize and handle.[75] A methoxy group at the position *para* to the nitrogen not only increases the electron donating strength of diarylamines, but enables reversible oxidations.[75,76] In contrast, materials with low LUMO energies, such as $mes_2B–(C_4H_2S)_n–Bmes_2$ (n = 2, 3; mes = 2,4,6-$Me_3C_6H_2$), are useful for electron transport.[77,78] Diarylboryl groups have attracted much interest for use in optoelectronic materials, as the vacant p_z-orbital of the three-coordinate boron serves as a strong π-acceptor, interacting with an adjacent π-system.[79–91] This conjugation provides the electron-deficient character that gives rise to useful photophysical properties.[92–94] For example, attaching a $Bmes_2$ moiety to the 2- and 2,7-positions of pyrene leads to a switch of the energetic order of the LUMO+1 and LUMO, which is a consequence of the mixing of the empty p_z-orbital with the pyrene B_{3u} LUMO+1. This mixing leads to a strong stabilization of the LUMO+1 such that it drops below the LUMO in energy.[95–97] Kinetic stabilization by bulky groups, such as mesityl or 2,4,6-$(CF_3)_3C_6H_2$ (Fmes), sterically protects the empty p_z-orbital from nucleophilic attacks leading to air- and moisture stable materials.[79–81,98,99] Incorporation of the boron into a rigid and planar structure is an alternative method to provide increased stability *via* structural constraints.[100]

With the above issues in mind, we were motivated to use the Ir-catalyzed C–H borylation reaction[45] to prepare new compounds in order to study the effect of strong π-donors and -acceptors at the 2,5,8,11-positions of perylene. We report herein the photophysical and electrochemical properties of the target compounds **$(Bmes_2)_4$-Per** and **$(DPA)_4$-Per**, which were examined experimentally and theoretically.

Results and discussion

Synthesis and structural characterization

The synthesis of the compounds **$(Bmes_2)_4$-Per** and **$(DPA)_4$-Per** is summarized in Scheme 1. The starting point of our approach is the high yielding Ir-catalyzed borylation of perylene, which we previously reported in 2005, providing **$(Bpin)_4$-Per** in 90% yield.[45] This synthesis is very convenient, as it can be run on a multigram scale and the tetra-borylated product does not need further purification, such as column chromatography, because the product crystallizes directly from the reaction solution. Suzuki–Miyaura cross-couplings with **$(Bpin)_4$-Per** have

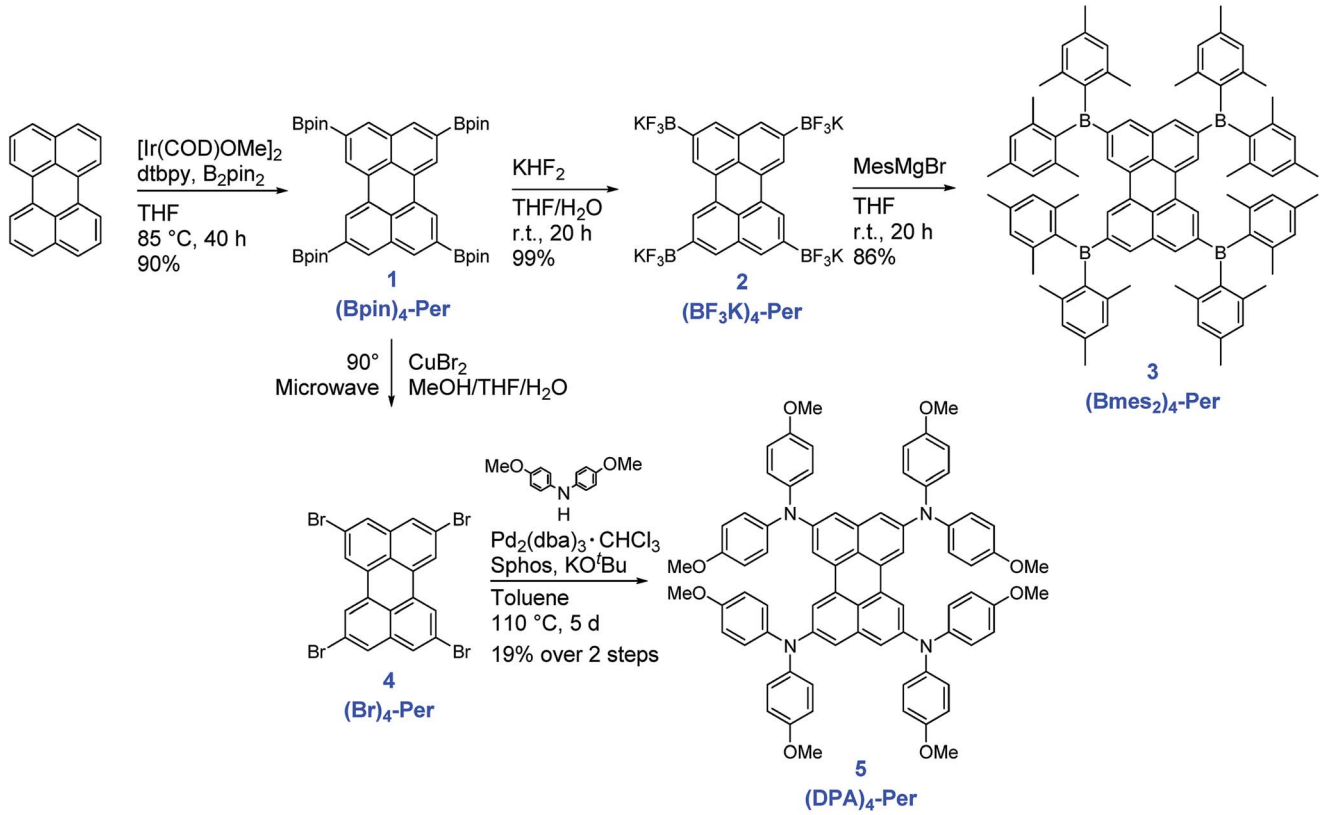

Scheme 1 Synthesis of the compounds $(Bpin)_4$-Per, $(BF_3K)_4$-Per, $(Bmes_2)_4$-Per, $(Br)_4$-Per and $(DPA)_4$-Per.

been reported before.[51,52] We, on the other hand, transformed this precursor into its potassium trifluoroborate salt **$(BF_3K)_4$-Per**. The synthesis was carried out in air in a THF/water mixture giving a yield of 99%. Potassium trifluoroborate salts are air- and moisture stable, and easy to handle and purify.[101,102] Furthermore, they can function as carbon nucleophiles and are important intermediates in diverse synthetic reactions.[103–105] However, they can also serve as boron electrophiles. Thus, **$(BF_3K)_4$-Per** reacts with the Grignard reagent mesMgBr to give **$(Bmes_2)_4$-Per** in 86% yield. Marder and co-workers previously demonstrated the utility of this approach to derivatize pyrene with a ($Bmes_2$) moiety.[106] Additionally, boroles were prepared from aryl trifluoroborates and aryllithium reagents.[99] The utility of a BF_3K salt as a boron electrophile for the synthesis of triarylboranes has also been demonstrated by Wagner and co-workers using aryllithium instead of Grignard reagents.[107,108]

The precursor **$(Bpin)_4$-Per** can also be transformed into the corresponding halogenated **$(Br)_4$-Per** by a halodeboronation.[109,110] Thus, **$(Bpin)_4$-Per** and $CuBr_2$ were suspended in a mixture of THF/MeOH/H_2O (1 : 1 : 1) and the reaction mixture was irradiated in a microwave reactor at 90 °C for 20 h. We note that performing this reaction in an oil bath instead of a microwave reactor results in a mixture of **$(Br)_3$-Per** and **$(Br)_4$-Per** as some protodeborylation occurs. Bromodeborylation of the C–Bpin bond is especially useful as it converts a carbon nucleophile into a carbon electrophile in one easy step. Thus, the **$(Br)_4$-Per** building block is a further useful intermediate that can serve in numerous types of coupling reactions including a Buchwald–Hartwig amination, which we performed to obtain **$(DPA)_4$-Per**. The fourfold amination of **$(Br)_4$-Per**, using $Pd_2(dba)_3\cdot CHCl_3$ as the catalyst precursor and Sphos as the ligand, was achieved in an overall yield of 19% in two steps starting from **$(Bpin)_4$-Per**. **$(DPA)_4$-Per** exhibits very good solubility in common organic solvents. The new products **2–5** were fully characterized by multinuclear NMR spectroscopy, high-resolution mass spectrometry, and elemental analysis.

The solid-state structure of **$(DPA)_4$-Per** was determined *via* single-crystal X-ray diffraction. The molecule shows inversion symmetry. In **$(DPA)_4$-Per**, the individual bond lengths are similar to those of perylene (Table S2†).[30] The naphthalene units of the perylene moiety exhibit typical aromatic C–C bond lengths ranging from 1.371(3) to 1.426(3) Å (Fig. 3a and Table S2†). The b and f bonds (1.371(3)–1.380(3) Å) are considerably shorter than the a, c, d, and e bonds (1.412(3)–1.426(3) Å) which is also observed in naphthalene and perylene.[31] The length of the C11–C13 bond (Fig. 3a, bond g, Table S2†) connecting the naphthalene units in **$(DPA)_4$-Per** is 1.470(2) Å at 100 K (Fig. 3). This is in the same range as the related bond distances reported for the two polymorphs of perylene (1.462–1.480 Å)[25–28,30,111] and, hence, resembles a $C(sp^2)$–$C(sp^2)$ single bond.[29–31]

The perylene core of **$(DPA)_4$-Per** is only slightly twisted with a small C10–C11–C13–C14 dihedral angle of 6.7(3)° (Fig. 3a and b). Crystal structures of perylene and *peri*-substituted perylenes in general show nearly planar perylene cores. For example,

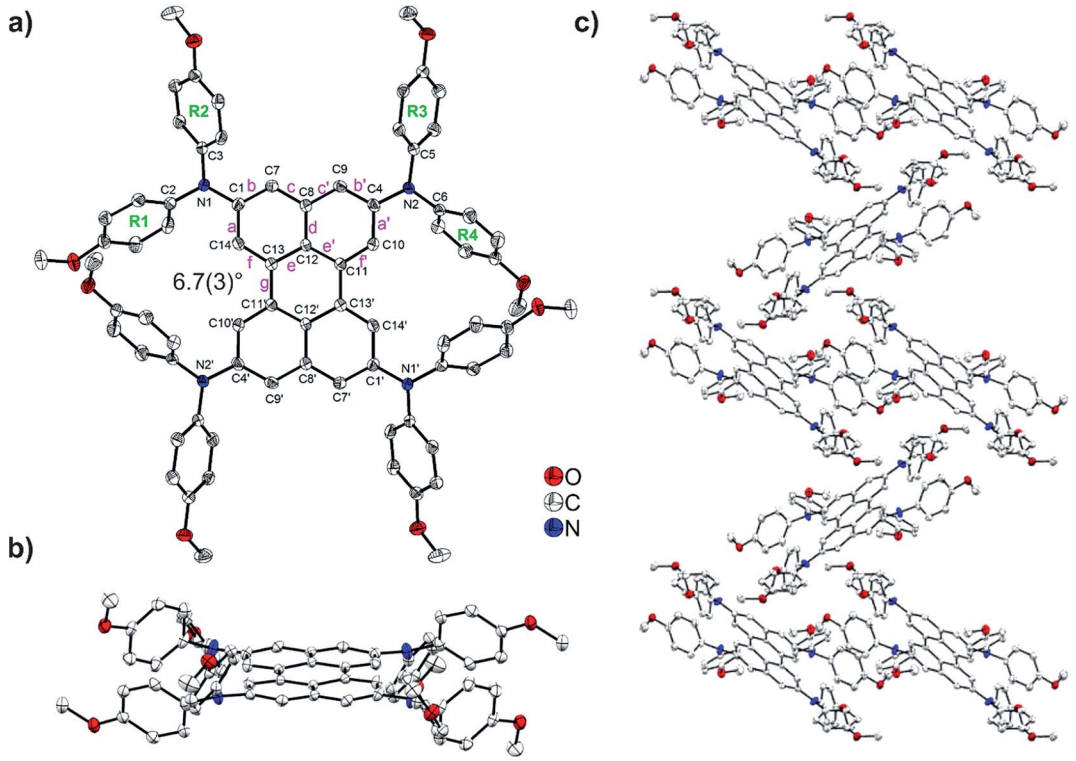

Fig. 3 Molecular structure of **(DPA)$_4$-Per**: (a) top view; (b) side view; and (c) packing of **(DPA)$_4$-Per** molecules. Hydrogen atoms are omitted for clarity. Element color: carbon (white), nitrogen (blue), oxygen (red). Atomic displacement ellipsoids are shown at the 50% probability level.

dihedral angles in the range 0.1–1.8° were reported for β- and α-perylene.[26–28,30,111,112] This shows that the substitution of the sterically demanding DPA moieties at the four *ortho* positions does not significantly affect the planarity of the perylene core. The nitrogen atoms are virtually trigonal planar with the sum of the angles around N1 being 359.8(2)° and N2 being 359.2(2)°, respectively. The interplanar angles between the terminal phenyl rings bonded to nitrogen and the NC_3 planes are 42.9–44.2° for R1, R2, and R3, and 66.0° for R4 (Fig. 3a, Table S2†). In contrast, the crystal structures of most of the perylene compounds containing *bay* substituents show a strong twist between the naphthalene units of the core due to steric repulsion created by the *bay* moieties.[44,113] For example, dihedral angles of 30.7–34.3° between the two naphthalene units have been reported for *bay*- and *ortho*-octasubstituted perylenes by Zeng and co-workers.[44] The packing of the **(DPA)$_4$-Per** molecules in the crystal structure is determined by the large steric demand of the amine moieties. There is no π–π stacking interaction present. Between the methoxy groups of the R1 and R4′ phenyl rings, and their inversion-related groups, intramolecular C–H···O interactions exist (Table S3†). Intermolecular C–H···C, C–H···π, and C–H···O interactions are present between methoxy groups, phenyl rings, and the perylene core. They are listed in detail in Table S3.† A Hirshfeld surface analysis was performed in order to quantify the nature and type of intermolecular interactions.[114–117] Fingerprint analysis and its breakdown to the individual relative contributions,[118–120] shows a major contribution from H···H interactions (59%), followed by a significant amount from C···H (29%) and O···H (10%) interactions, and minor contribution of O···C interactions (1%). Only very weak contributions (<1%) from C···C, O···O, and N···H interactions are observed (Fig. S28 and S29†).

Photophysical properties

The absorption spectra of **(Br)$_4$-Per** and **(Bpin)$_4$-Per** are generally very similar to that of perylene. Their $S_1 \leftarrow S_0$ transition, which is *z*-axis polarized (L_a) and basically attributed to a HOMO → LUMO transition, is allowed with extinction coefficients of 28 000–32 000 M^{-1} cm^{-1} (perylene: 34 000 M^{-1} cm^{-1}). Furthermore, this band has a well-defined vibronic fine structure with an interval of 1400 cm^{-1} between the sub-bands as in perylene. However, it is slightly bathochromically shifted (310 cm^{-1} for **(Bpin)$_4$-Per** and 360 cm^{-1} **(Br)$_4$-Per**) with respect to the parent perylene. Thus, the $S_1 \leftarrow S_0$ transition in these derivatives is a pure π → π* transition. As observed previously on pyrene,[106] the Bpin moieties barely influence the photophysical properties of perylene, as oxygen substituents at the boron atom decreases its π-acceptor properties.[121] Bromo substituents are only weak π-donors; therefore, these two derivatives show hardly any CT character. This is consistent with the observed absorption properties reported for bromo-substituted PDI's.[122] It is interesting to observe that, in comparison with the 2,5,8,11-tetrabromo-1,6,7,12-tetra-*n*-butoxyperylene reported by Zeng and co-workers,[44] the $S_1 \leftarrow S_0$ transition of **(Br)$_4$-Per** is narrower, structurally better defined and, furthermore, slightly more allowed.[123] This indicates some

influence of the donating *bay* substituents on the absorption properties. However, there are no previous reports on perylene derivatives substituted only at the *ortho* positions for comparison. Stronger π-accepting moieties, such as $Bmes_2$, at the *ortho* positions leads to a pronounced influence on the $S_1 \leftarrow S_0$ transition. Hence, the lowest energy band in **$(Bmes_2)_4$-Per** is much broader and is strongly bathochromically shifted (1220 cm^{-1}) with respect to the L_a band of perylene which indicates a stabilization of the unoccupied orbitals of this derivative in comparison to those of perylene (*vide infra*).

Furthermore, this transition is much less allowed with an extinction coefficient of 20 000 M^{-1} cm^{-1}. However, this band still possesses a vibronic fine structure, but the modes have rather similar intensity. In comparison to the acceptor version reported by Zeng and co-workers[44] (2,5,8,11-tetracyano-1,6,7,12-tetra-*n*-butoxyperylene) (λ_{max}(abs) = 454 nm) the absorption of **$(Bmes_2)_4$-Per** is further bathochromically shifted (λ_{max}(abs) = 465 nm), which indicates a stronger stabilization of the unoccupied orbitals in our derivative. We have previously shown[48,95–97] that CN is a less effective π-acceptor than $Bmes_2$ when attached to pyrene. The influence on the $S_1 \leftarrow S_0$ transition is even more pronounced in **$(DPA)_4$-Per** as it does not have any vibrational progression. Its L_a band is broader and more strongly bathochromically shifted with respect to the L_a band of perylene (2690 cm^{-1}) than for **$(Bmes_2)_4$-Per**. Hence, the donor DPA substituents exert a larger destabilizing effect on the occupied frontier orbitals than the acceptor $Bmes_2$ stabilizes the empty ones. This is similar to what we observed for 2,7-pyrene derivatives.[106] Both target derivatives, **$(Bmes_2)_4$-Per** and **$(DPA)_4$-Per** have the lowest energy absorptions reported so far for *ortho* substituted perylene derivatives.

All derivatives show intense fluorescence in the blue to orange region of the electromagnetic spectrum with quantum yields Φ of up to 0.58 (Fig. 4, Table 2). The emission spectra of **$(Br)_4$-Per** and **$(Bpin)_4$-Per** are very similar to that of perylene, in that the apparent Stokes shifts[124] are very small (300–350 cm^{-1}) and the band shape is a mirror image of its respective $S_1 \leftarrow S_0$ absorption. The radiative rate constants of both **$(Br)_4$-Per** and **$(Bpin)_4$-Per** are the same order of magnitude ($k_r = 12 \times 10^7$ s^{-1}) as that of perylene. Thus, their excited state structures are presumably very similar to those in the ground state. It is interesting to note that 2,5,8,11-tetrabromo-1,6,7,12-tetra-*n*-butoxyperylene displays a broad emission without vibronic fine structure and a significantly larger apparent Stokes shift of 2120 cm^{-1}, indicating modest geometry changes in its excited state. Furthermore, its emission quantum yield of $\Phi = 0.30$ is only half that of **$(Br)_4$-Per** ($\Phi = 0.58$) but, as Zeng and co-workers did not report lifetimes or radiative decay rates, a full comparison is not possible. The differences observed must be a result of the *bay* substituents that lead to a twisted core.[126] The significant influence of *bay* substituents on the photophysical properties of PDI's such as enhanced nonradiative decay was already reported by several groups.[13,113,122,127,128] Nevertheless, for PAHs with heavy atoms such as Br, the emissions we measured are intense, and no phosphorescence was detected at 77 K. However, Dreeskamp and Koch already reported[129,130] that the bromination of perylene at its *peri* position (*i.e.* 3-bromoperylene) does not lead to a quenching of the fluorescence by intersystem crossing (ISC) from S_1 *via* spin–orbit coupling. They found that the energy gap between the S_1 and T_1 of 3-bromoperylene is not small enough for ISC to compete with fluorescence. Furthermore, Hariharan and co-workers demonstrated that the bromination of PDIs also fails to promote ISC and, even in dibromoethane solutions, no effect of the external heavy atoms on ISC was observed.[131]

The emission of **$(Bmes_2)_4$-Per**, with λ_{max}(em) = 489 nm, is bathochromically shifted by 2073 cm^{-1} in comparison to that of perylene and thus has a larger apparent Stokes shift of 1055 cm^{-1}. Its intense emission (quantum yield $\Phi = 0.43$) shows vibronic fine structure in toluene, which does not vanish in THF. Furthermore, this derivative shows no solvatochromism which indicates the absence of charge transfer (CT) character. In the solid state, a green emission with λ_{max}(em) = 525 nm is observed, but the non-radiative decay rate k_{nr} is greatly enhanced by more than one order of magnitude ($k_{nr} = 79 \times 10^7$ s^{-1}), which leads to a decreased quantum yield. However, emission in the solid state is rather uncommon for perylene derivatives. The fluorescence of PDIs, for instance, is quenched in the solid state on account of H-type aggregation due to π–π interactions.[132] The emission of the donor-substituted derivative **$(DPA)_4$-Per** is further bathochromically shifted (λ_{max}(em) = 569 nm), shows no vibronic fine structure and is very broad. Furthermore, it exhibits significant solvatochromism, confirming a pronounced CT character. The large apparent Stokes shift (3 100 cm^{-1} in THF) is untypical for perylenes, as PDIs usually have very small apparent Stokes shifts. However, a large apparent Stokes shift helps to reduce self-quenching and thus to avoid measurement errors.[35] The excited state of **$(DPA)_4$-Per** has an intrinsic lifetime of $\tau_0 = 46$ ns and is thus significantly longer lived than perylene ($\tau_0 = 4$ ns) and is highly stabilized in a polar environment, as in THF $\tau_0 = 94$ ns. The radiative decay rates k_r of the target compounds **$(DPA)_4$-Per** ($k_r = 2.2 \times 10^7$ s^{-1}) and **$(Bmes_2)_4$-Per** ($k_r = 6.5 \times 10^7$ s^{-1}) are one order of magnitude slower than of perylene ($k_r = 24 \times 10^7$ s^{-1}) which is in full agreement with the Strickler–Berg relationship[133] as the $S_1 \leftarrow S_0$ transition of these derivatives is also less allowed. The **$(DPA)_4$-Per** derivative has the slowest radiative decay which is also in full agreement with the Strickler–Berg relationship[133] as its emission is further bathochromically shifted. Interestingly, substituting one DPA moiety at a *peri* position of perylene results in two emissions at λ_{max}(em) = 530 nm and 630 nm, respectively, while further studies showed[125] that the dual emission results from two excited state rotamers with different angular distribution. However, emission from the *peri*-substituted derivative proceeds significantly faster with radiative decay rates of $k_r = 8.8 \times 10^7$ s^{-1}.[125] Hence, substituents at the *ortho* positions have a distinctly different influence on the excited state properties than substituents at the *peri* positions.

Reactivity with oxygen

In 1974, Dreeskamp, Koch and co-workers showed that the rate of ISC from the fluorescent singlet to a triplet state can be increased in perylene by an intermolecular energy transfer to

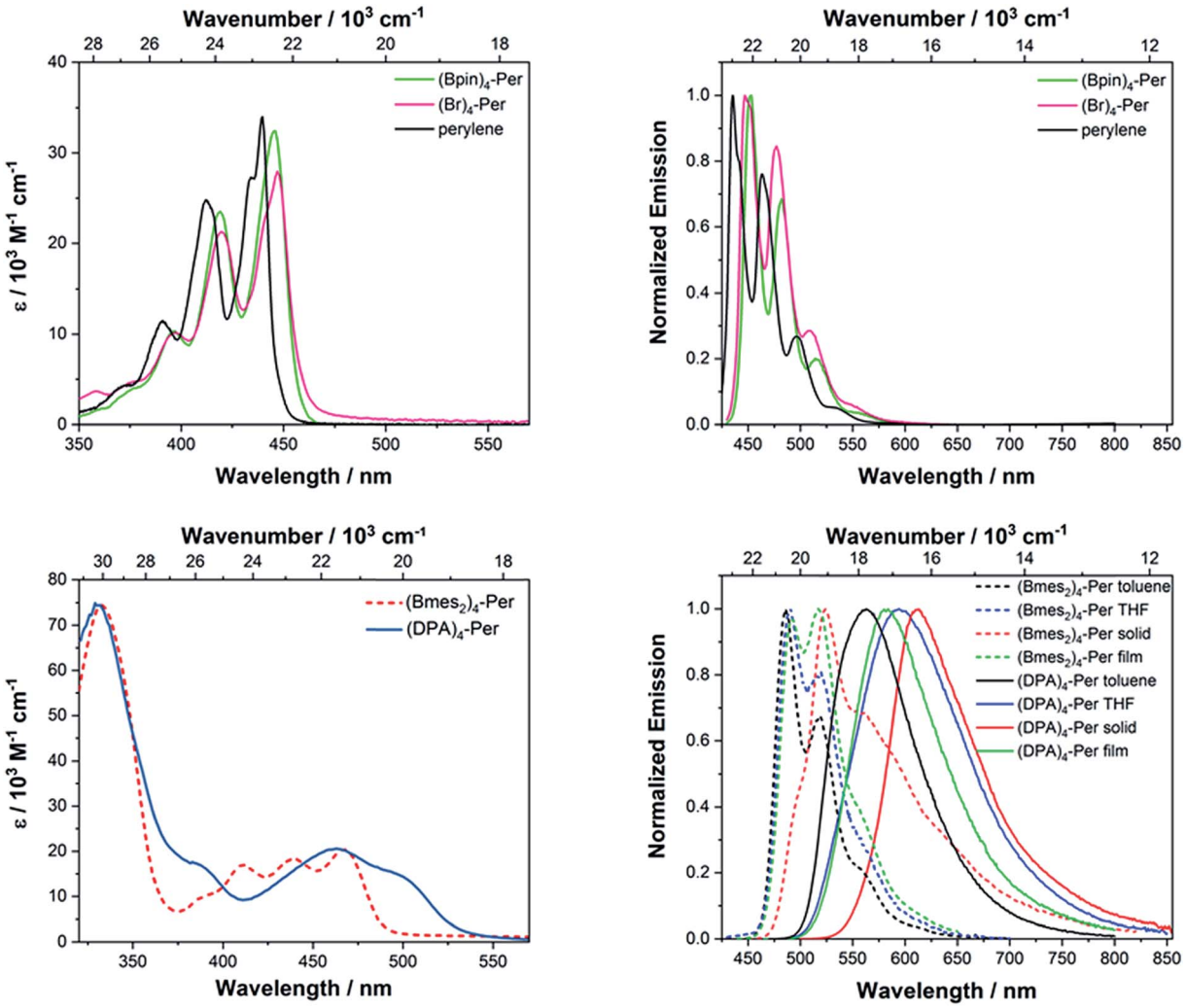

Fig. 4 Absorption (left) and emission (right) spectra of $(Br)_4$-Per and $(Bpin)_4$-Per (top) and $(Bmes_2)_4$-Per and $(DPA)_4$-Per (bottom) recorded in toluene if not otherwise noted.

halogenated-naphthalene.[129,130,134] This precedence motivated us to take a closer look at our systems as the fluorescence quantum yield of **$(DPA)_4$-Per** is particularly low ($\varphi = 0.26$) compared to perylene and triplet sensitizers are of great interest with many applications in phosphorescent materials,[135–137] phosphorescent bioimaging,[135,137,138] chemosensors,[135,137,139] photoinitiated polymerization,[137,140] photocatalysis,[137,141–144] triplet–triplet annihilation based upconversion,[137,145,146] and oncological or antibacterial photodynamic therapy.[137,147,148] There are a few reports on triplet states of PDIs and these make use of bimolecular triplet sensitization,[149] incorporation of sulfur[150] or heavy metals such as Ir,[131,151,152] Pt,[153] Pd,[152,154] or Ru.[152] Flamigni and co-workers demonstrated[155,156] that unsymmetrical substitution of PDIs is an alternative method to access triplet states. Furthermore, in 2016, Hariharan and co-workers reported[131] that, through heavy atom substitution combined with a twisted-core structure of PDIs, triplet states of PDIs become accessible. One indication for an enhanced ISC rate is energy transfer from the triplet state of a compound formed upon photoexcitation to ground state oxygen ($^3\sum_g^-$). This leads to the generation of singlet oxygen ($^1\Delta_g$), which can be detected by its luminescence at 1272 nm. Accordingly, upon excitation of an O_2-saturated toluene solution of **$(DPA)_4$-Per**, an emission at 1272 nm was detected (Fig. 5).

Compared to the standard, perinaphthenone, for which the quantum yield of $^1\Delta_g$ production is close to unity,[157] **$(DPA)_4$-Per** sensitizes $^1\Delta_g$ with a quantum yield of 0.60. On the other hand, the derivative **$(Bmes_2)_4$-Per** does not sensitize $^1\Delta_g$ to any measurable extent. However, as the singlet excited state of **$(DPA)_4$-Per** is long-lived ($\tau = 12$ ns, $\varphi = 0.26$) and quenched in an O_2-saturated solution ($\tau = 4.6$ ns, $\varphi = 0.09$), it is reasonable that the formation of $^1\Delta_g$ is not only a product of its triplet state but also of the singlet excited state.[158,159] McLean and co-workers reported that perylene sensitizes $^1\Delta_g$ with a quantum yield of 0.65 in an oxygen-saturated benzene solution even though formation of its triplet state has a vanishing quantum yield, thus, implying $^1\Delta_g$ sensitization from its excited singlet state only.[159,160] However, as for **$(DPA)_4$-Per** the yield of sensitized $^1\Delta_g$ is larger than the fluorescence quantum yield, a significant part must be sensitized from its triplet state. To confirm this, we

Table 2 Selected photophysical data of perylene and its derivatives **(Bpin)$_4$-Per**, **(Br)$_4$-Per**, **(Bmes$_2$)$_4$-Per** and **(DPA)$_4$-Per** recorded under argon at room temperature if not otherwise noted

Cpd	Medium	λ_{abs}/nm (ε/10^3 M^{-1} cm^{-1})	λ_{em}[a]/nm	Apparent Stokes[124] shift/cm^{-1}	τ[b]/ns	τ_{avg}[c]/ns	Φ	τ_0/ns	k_{nr}/10^7 s^{-1}	k_r/10^7 s^{-1}
Perylene[d]	Toluene	440 (34)	444	4	4.0	—	0.95	4.0	1.3	24
(Bpin)$_4$-Per	Toluene	446 (32), 419 (24), 397 (10)	453	350	4.9	—	0.58	8.0	8.6	12
(Br)$_4$-Per	Toluene	447 (28), 420 (21), 397 (10)	453	300	4.7	—	0.55	9.0	9.6	12
(Bmes$_2$)$_4$-Per	Toluene	465 (20), 440 (18), 412 (17), 333 (74)	489	1060	6.6	—	0.43	15	8.6	6.5
	THF	466, 441, 412, 335	489	1010	8.6	—	0.41	21	6.7	4.8
	Solid	—	525	—	0.9 (87) 3.6 (13)	1.2	0.04	31	79	3.2
	Film[f]	—	490, 517	—	7.3 (87) 13 (13)	8.0	0.36	22	8.0	4.5
(DPA)$_4$-Per	Toluene	499 (15), 463 (20), 386 (17), 331 (74)	569	2470	12	—	0.26	46	6.2	2.2
	Toluene[e]	—	569	—	4.6	—	0.09	51	20	2.0
	THF	501, 459, 383, 327	593	3100	8.5	—	0.09	94	11	1.1
	Solid	—	612		2.5 (67) 6.4 (33)	3.8	0.07	54	26	1.9
	Film	—	580	—	12 (86) 20 (14)	13	0.14	92	6.7	1.1

[a] Excited at the respective λ_{abs} (max) of $S_1 \leftarrow S_0$. [b] Pre-exponential factors B_n scaled to 100 and given in parentheses. [c] For multi-exponential decays the pure radiative lifetime $\tau_0 = \tau/\Phi$ has been approximated by using the experimental average lifetime $\tau = \sum\tau_n B_n / \sum B_n$ with B_n being the pre-exponential factors of the respective lifetime component τ_n. [d] From Brites and co-workers.[125] [e] In an O_2-saturated solution. [f] PMMA film doped with 1% of the respective perylene derivative.

performed transient absorption measurements on **(DPA)$_4$-Per** in order to investigate a possible triplet state. Indeed, excited state absorption in the range 400–710 nm was observed revealing a long-lived excited state with a lifetime of 500 μs, which is completely quenched in an O_2-equilibrated solution (Fig. S3†).

Electrochemistry

Cyclic voltammetry studies on **(Bmes$_2$)$_4$-Per** revealed four reversible reductions occurring at −2.04 V, −2.45 V, −2.79 V and −2.98 V with respect to Fc/Fc$^+$ (in THF) to its anion, dianion, trianion and tetraanion, respectively, as shown in Fig. 6 and Table 3. The first reduction is not significantly shifted while the second, third and fourth reductions are cathodically shifted by 0.38 V, 0.72 V and 0.91 V, respectively, compared to the first reduction of perylene.[37] The fourth reduction is cathodically shifted by 0.32 V compared to the second reduction of perylene. However, **(Bmes$_2$)$_4$-Per** shows stability towards very high reduction potentials with the advantage that it has a high electron capacity, as up to four electrons can be stored. This intriguing property is interesting for applications including molecular switches,[161,162] receptors,[162,163] photoactive dyads[164] or photocatalysis.[143,165]

The donor-substituted counterpart, **(DPA)$_4$-Per**, can be oxidized up to five times according to cyclic voltammetry studies

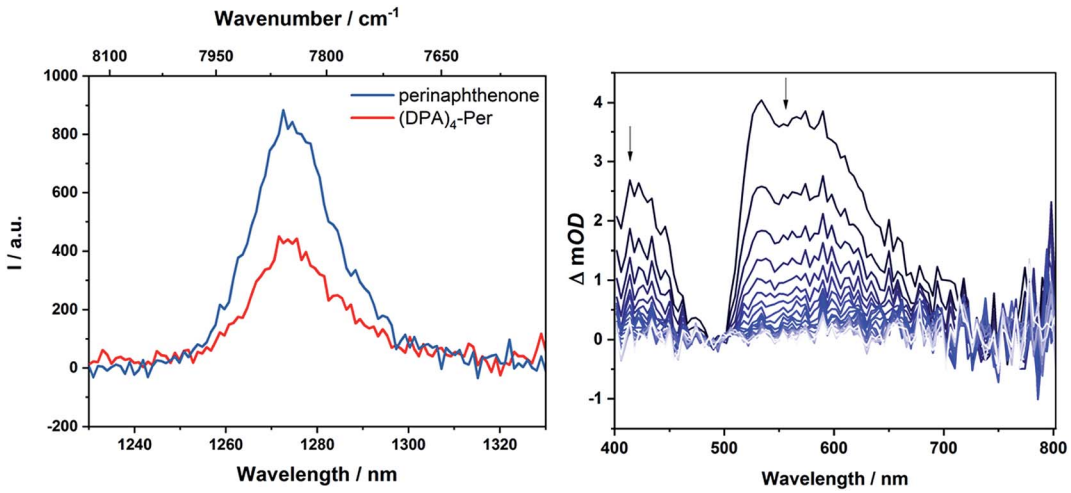

Fig. 5 Singlet oxygen luminescence from optically matched toluene solutions of **(DPA)$_4$-Per** and the standard perinaphthenone; excitation at 340 nm (left); nanosecond transient absorption spectrum of **(DPA)$_4$-Per** in a degassed DMF solution (right) at intervals of 169.9 μs.

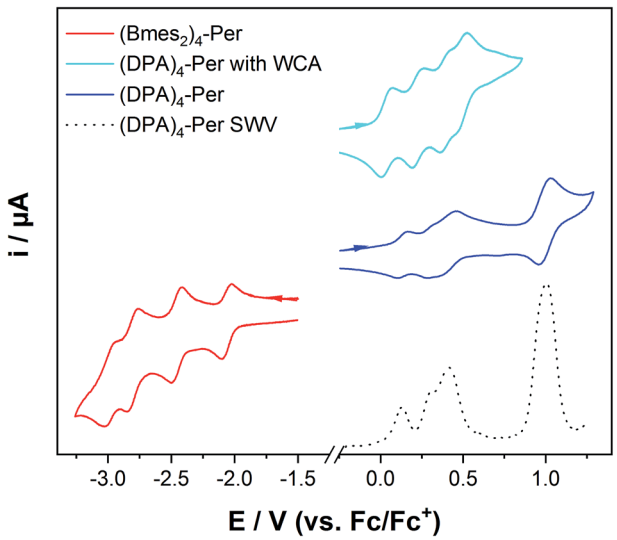

Fig. 6 Cyclic voltammograms of **(Bmes$_2$)$_4$-Per** in THF/0.1 M [*n*-Bu$_4$N][PF$_6$] at 500 mV s^{-1} (red) and **(DPA)$_4$-Per** in CH_2Cl_2/0.1 M [*n*-Bu$_4$N][PF$_6$] (blue), and CH_2Cl_2/0.1 M [Al(O(CF$_3$)$_3$)$_4$][*n*-Bu$_4$N] (cyan), respectively, at 250 mV s^{-1}, and a square wave voltammogram (dashed line) of **(DPA)$_4$-Per** in CH_2Cl_2/0.1 M [*n*-Bu$_4$N][PF$_6$].

in CH_2Cl_2/0.1 M [*n*-Bu$_4$N][PF$_6$]. The first two oxidations are well separated, but the second, third and fourth oxidations are very close to one another and hard to quantify. Therefore, we performed square-wave voltammetry measurements which are known to be more sensitive than cyclic voltammetry.[166,167] The first two oxidations are again well separated occurring at 0.13 V and 0.31 V, the third oxidation occurs at 0.41 V and the larger signal intensity of the latter indicates a fourth oxidation within this area. A further oxidation at 0.98 V occurs which is possibly due to the methoxy moieties. We performed a further cyclic voltammetry study using the weakly coordinating anion (WCA)-containing electrolyte [*n*-Bu$_4$N][Al(OC(CF$_3$)$_3$)$_4$].[168] WCAs are known to separate charged species in electrochemical studies better and thus give a larger potential splitting.[169] Thus, four clear, reversible oxidations at 0.040 V, 0.24 V, 0.41 V and 0.51 V to the radical cation, dication, radical trication and tetracation, respectively, of **(DPA)$_4$-Per** were observed, whereas the fifth oxidation is not reversible in this electrolyte.

These numerous reductions and oxidations of our two derivatives are remarkable for perylenes, because PDIs only possess up to two reductions or oxidations and a fourfold reduction has only been reported for bi(PDI)s.[170–173] PAHs that can be reduced or oxidized multiple times are rare, with the typical example being fullerenes.[174] A recent report by Oki *et al.* indicated that a pyrrole-fused azacoronene analogue could be reversibly oxidized four times, which was also observed for hexapyrrolohexaazacoronenes.[175,176] Nevertheless, the *bay* and *ortho* octa-substituted perylenes reported by Zeng and co-workers[44] show only a maximum of two oxidations at 0.42 V and 0.72 V in CH_2Cl_2/0.1 M [*n*-Bu$_4$N][PF$_6$] for the derivative with four methoxy moieties at the *ortho* positions (2,5,8,11-tetramethoxy-1,6,7,12-tetra-*n*-butoxyperylene) *vs.* Fc/Fc$^+$. These oxidations are significantly shifted to higher potentials compared to **(DPA)$_4$-Per**. Hence, our donor substituted perylene derivative is among the most electron-rich perylenes reported to date, and the HOMO of **(DPA)$_4$-Per** must be strongly destabilized, which is unique for perylenes as they usually have very poor electron-donating abilities.[177] The compound 2,5,8,11-tetracyano-1,6,7,12-tetra-*n*-butoxyperylene has only one irreversible reduction at −1.63 V in CH_2Cl_2/0.1 M [*n*-Bu$_4$N][PF$_6$]. Thus, Bmes$_2$ as an acceptor at the *ortho* positions of perylene enables the possibility of multiple reductions, in contrast to the cyano acceptor.[44]

To investigate the properties of the radical cation, dication, radical trication and tetracation of **(DPA)$_4$-Per** we performed UV/Vis/NIR spectrochemical measurements in CH_2Cl_2/0.1 M [*n*-Bu$_4$N][Al(OC(CF$_3$)$_3$)$_4$]. However, due to the small redox-potential separations, it was not possible to generate exclusively each charged species. Nevertheless, the radical mono-cation can be observed as the "nearly pure" cation without further deconvolution, and is depicted in Fig. 7, while all further spectra are given in the ESI (Fig. S3–S6†). Upon oxidation to the radical mono-cation a very broad and symmetric transition appears between 2400 and 8000 cm^{-1} with a maximum at $\tilde{\nu}_{max}^{IVCT}$ = 3813 cm^{-1} (2 622 nm, ε = 9 900 M^{-1} cm^{-1}) in the NIR. The transition at *ca.* 1100 nm appears at higher oxidation potentials and thus belongs to the dication (Fig. S6†). The analysis of this intervalence charge-transfer band (IV-CT) according to the Mulliken–Hush theory is straightforward as DFT calculations (see below) reveal a vanishing dipole moment difference between ground and excited state upon excitation.[178,179] Thus, the radical cation is a delocalized Robin-Day-class-III mixed valence (MV) compound and the electronic coupling between the two diabatic redox states can be evaluated as one half of the energy of the absorption maximum.[180–184]

$$V = \frac{\tilde{\nu}_{max}^{IVCT}}{2} \quad (1)$$

In this way we evaluated V to be 1807 cm^{-1} as half of the IV-CT excitation energy (β-HOMO → β-LUMO). This result is fully

Table 3 Cyclic voltammetry results for **(Bmes$_2$)$_4$-Per** in THF/0.1 M [*n*-Bu$_4$N][PF$_6$] and **(DPA)$_4$-Per** in CH_2Cl_2/0.1 M [*n*-Bu$_4$N][PF$_6$] relative to the Fc/Fc$^+$ couple if not otherwise noted

	$E_{1/2}$ [V] [red]^1	$E_{1/2}$ [V] [red]^2	$E_{1/2}$ [V] [red]^3	$E_{1/2}$ [V] [red]^4	$E_{1/2}$ [V] [ox]^1	$E_{1/2}$ [V] [ox]^2	$E_{1/2}$ [V] [ox]^3	$E_{1/2}$ [V] [ox]^4
(Bmes$_2$)$_4$-Per	−2.04	−2.45	−2.79	−2.98	—	—	—	—
(DPA)$_4$-Per	—	—	—	—	0.13	0.31	0.41	0.98
(DPA)$_4$-Per with WAC[a]	—	—	—	—	0.040	0.24	0.41	0.51

[a] Measured in CH_2Cl_2/0.1 M [*n*-Bu$_4$N][Al(OC(CF$_3$)$_3$)$_4$] relative to the Fc/Fc$^+$ couple.

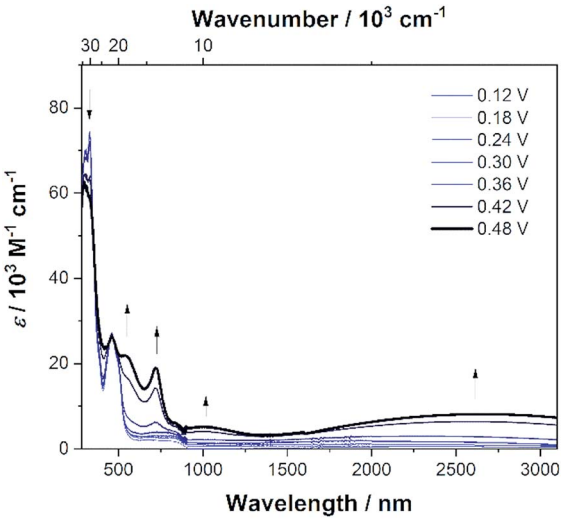

Fig. 7 Spectroelectrochemical measurements of the stepwise oxidation process of **(DPA)$_4$-Per** in CH_2Cl_2/0.1 M [*n*-Bu_4N][$Al(OC(CF_3)_3)_4$]. The absorption spectrum of **(DPA)$_4$-Per$^+$** is shown as a solid black line.

in line with the TD-DFT computations of the radical monocation that we performed as the orbitals involved in the excitation show the expected phase behavior for a Robin-Day-class-III compound (Fig. 8, S36 and Table S4†). Unfortunately, it was not possible to evaluate the electronic coupling within the radical trication, because the redox-potential separations between the dication, radical trication and tetracation are too close to each other. Furthermore, **(Bmes$_2$)$_4$-Per** could not be studied by spectroelectrochemical measurements, as the absorption spectrum of the neutral species cannot be reproduced in intensity after the reductions (Fig. S8–S12†).

DFT and TD-DFT calculations

To rationalize the observed trends and properties, we performed DFT and TD-DFT studies on perylene, **(DPA)$_4$-Per**, and **(Bmes$_2$)$_4$-Per**. Furthermore, the model derivatives **(NH$_2$)$_4$-Per** and **(BH$_2$)$_4$-Per** were calculated and compared with perylene to understand how the frontier molecular orbitals of both compounds are related to the parent perylene system (Fig. S37–S39†). We optimized the ground-states in the gas-phase at the B3LYP/6-31G (d,p) level of theory. Previous studies[95,185] have shown that range-separated hybrid functionals are necessary to obtain a reliable picture of the nature and relative energetic ordering of the excited states. Therefore, the CAM-B3LYP functional was employed for the subsequent TD-DFT calculations for the perylene derivatives.

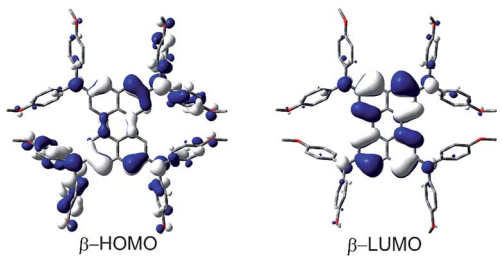

Fig. 8 Depiction of the β-HOMO and β-LUMO that are responsible for the lowest energy absorption (IV-CT band) of **(DPA)$_4$-Per$^+$**.

Perylene has a large HOMO–LUMO gap (3.05 eV) and its HOMO–1/HOMO and LUMO/LUMO+1 orbitals are well separated. Adding four Bmes$_2$ moieties to the *ortho* positions of perylene (**(Bmes$_2$)$_4$-Per**) leads to a 0.20 eV stabilization of the LUMO, which is a combination of the empty p_z orbitals of the boron atoms of the Bmes$_2$ fragments and the perylene LUMO resulting in larger orbital coefficients at the *ortho* positions compared to the parent perylene (Fig. 9).

Perylene's LUMO+1, LUMO+3 and LUMO+4 mix even stronger with the Bmes$_2$ fragments, which leads to an increased stabilization of their energies by 1.35 eV, 1.54 eV and 1.58 eV, respectively. Hence, these three orbitals above the LUMO, are all greatly stabilized in **(Bmes$_2$)$_4$-Per** and are close in energy. This is a plausible explanation for the four electron reduction of this compound that we observed within the cyclic voltammetry studies. The stabilization of the LUMO furthermore explains the observed bathochromic shift of the $S_1 \leftarrow S_0$ transition, which consists of a pure HOMO → LUMO transition. This contrasts strongly with 2,5,8,11-tetracyano-1,6,7,12-tetra-*n*-butoxyperylene, which shows that the cyano group does not mix as efficiently with the perylene LUMO and we already made this observation in a closely related pyrene derivative.[44,97] This is reflected in the photophysical behavior, as the $S_1 \leftarrow S_0$ transition of 2,5,8,11-tetracyano-1,6,7,12-tetra-*n*-butoxyperylene is not as bathochromically shifted as that of **(Bmes$_2$)$_4$-Per**. Nevertheless, this comparison should be treated with caution as the *bay* substituents certainly have some influence (*vide supra*). However, the calculations show that the LUMO is mainly distributed over the four boron centers and the perylene core while the mesityl moieties do not contribute to this orbital (Fig. 9). Even though there is some contribution of the Bmes$_2$ fragments to the LUMO and LUMO+1 to LUMO+3 of **(Bmes$_2$)$_4$-Per**, these orbitals generally resemble those in unsubstituted perylene. Therefore, the HOMO → LUMO transition of **(Bmes$_2$)$_4$-Per** does not have much CT character, and is predominantly a local excited state (LE), which agrees with our photophysical studies, as the emission spectrum of **(Bmes$_2$)$_4$-Per** does not show solvatochromism. The HOMO is not influenced by the Bmes$_2$ fragments and thus does not change much in energy. However, 16 orbitals, which are based on the mesityl fragments only, *i.e.*, are not affected by the perylene core or boron atoms, and form the HOMO−1 to HOMO−16 (Fig. 8, grey) of **(Bmes$_2$)$_4$-Per**. The former HOMO−1 through HOMO−4 are not altered by the Bmes$_2$ groups and now form the HOMO−17 to HOMO−20 (Fig. 8, black, blue, cyan and green).

In contrast, adding four amine donor moieties to the *ortho* positions of the perylene core destabilizes the occupied orbitals much more than the virtual ones. The nitrogen p_z orbitals of the DPA moieties mix very well with the occupied orbitals of the perylene core, but the π-orbitals of the methoxy phenyl rings also contribute significantly. The mixing of the perylene HOMO with N(p_z) and NAr_2 orbitals leads to two new perylene-like

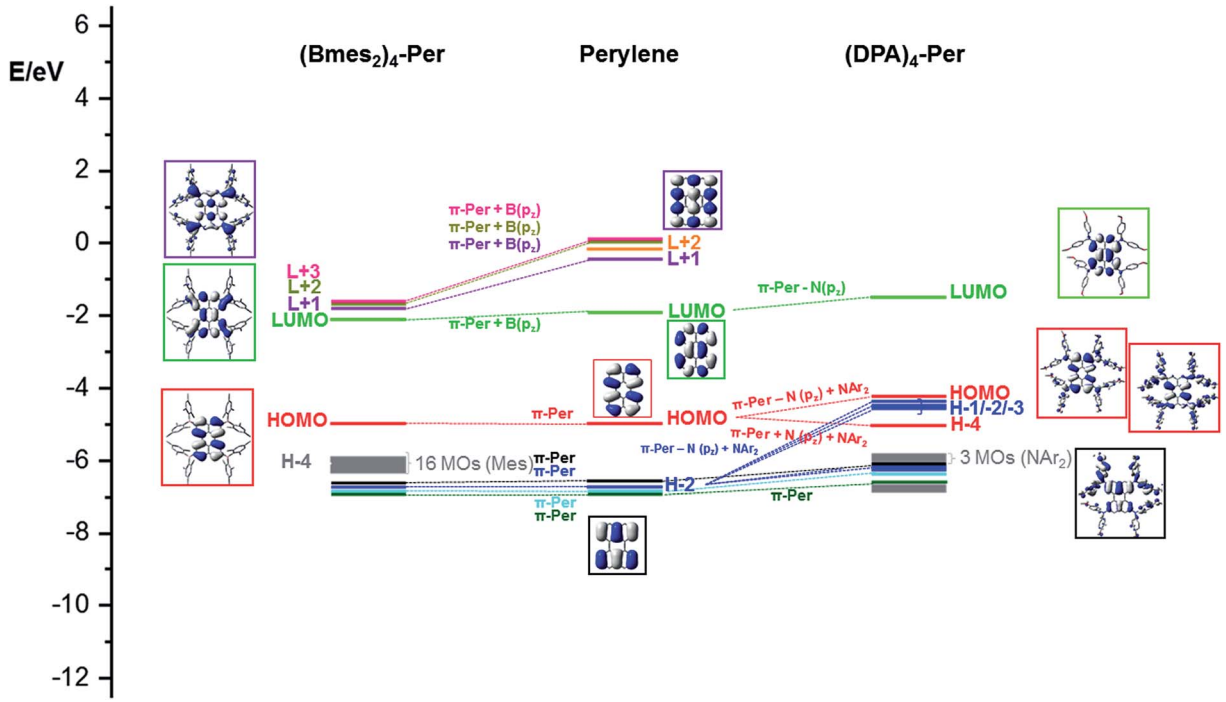

Fig. 9 Frontier MO-diagram (B3LYP/6-31+G(d,p)) and depiction of **B(mes$_2$)$_4$-Per** (left), **perylene** (middle) and **(DPA)$_4$-Per** (right) showing the relation between the frontier orbitals of perylene and its acceptor and donor substituted derivatives. The key frontier molecular orbitals are shown in color-coded boxes.

HOMOs in **(DPA)$_4$-Per** (HOMO and HOMO−4) (Fig. 8, red). The new HOMO of **(DPA)$_4$-Per** is strongly destabilized by 0.73 eV while HOMO−4 is slightly stabilized in comparison to the HOMO of perylene. In a similar manner, for HOMO−2 of perylene, two new sets are formed in **(DPA)$_4$-Per** (Fig. 8, blue). One set (HOMO−1 through HOMO−3) is strongly destabilized by *ca.* 0.79 eV and the second by *ca.* 0.59 eV (HOMO–9 and HOMO–10). Perylene's HOMO–1 to HOMO–3 and HOMO−4 (Fig. 9, black, cyan and green), on the other hand, are less destabilized in **(DPA)$_4$-Per.** These results agree with our observed photophysical properties. The strong destabilizing effect of the HOMO in **(DPA)$_4$-Per** explains the strong bathochromic shift of the $S_1 \leftarrow S_0$ transition and as the HOMO of **(DPA)$_4$-Per** is also distributed over the four amine moieties and displays a pronounced CT character, this is reflected in the broad and structureless absorption and emission spectra as well as the solvatochromic behavior. Thus, the effect of the DPA groups on the occupied orbitals of the perylene is more pronounced than is the case of the $Bmes_2$ moieties, where only the unoccupied orbitals were affected. Furthermore, the observed electrochemical behavior is

Table 4 TD-DFT results (CAM-B3LYP/6-31G (d,p)) for the five vertical transitions of perylene, **(Bmes$_2$)$_4$-Per** and **(DPA)$_4$-Per**

	FC-S_n	E [eV] (E [nm])	f	Configuration (major contributions > 10%)
Perylene	S_1	3.21 (387)	0.446	H → L (99%)
	S_2	4.06 (305)	0.000	H → L+1 (58%), H−1 → L (33%)
	S_3	4.34 (285)	0.004	H−2 → L (52%), H → L+3 (38%)
	S_4	4.45 (278)	0.000	H → L+2 (42%), H−4 → L (24%), H−1 → L (23%)
	S_5	4.88 (254)	0.000	H → L+2 (52%), H−4 → L (30%), H → L+1 (13%)
(Bmes$_2$)$_4$-Per	S_1	3.03 (410)	0.367	H → L (96%)
	S_2	3.21 (386)	0.000	H → L+1 (87%)
	S_3	3.54 (350)	0.212	H → L+3 (79%)
	S_4	3.64 (340)	0.000	H → L+2 (92%)
	S_5	4.01 (310)	0.055	H−4 → L+1 (21%), H−2 → L (20%), H−1 → L+2 (21%), H−3 → L+3 (16%)
(DPA)$_4$-Per	S_1	3.00 (413)	0.318	H → L (91%)
	S_2	3.11 (398)	0.017	H−1 → L (76%)
	S_3	3.30 (376)	0.281	H−2 → L (74%)
	S_4	3.48 (356)	0.005	H−3 → L (77%)
	S_5	3.92 (316)	0.294	H−4 → L (78%)

consistent with our calculations, as the influence on the occupied orbitals results in four orbitals that are very close in energy and around the HOMO of **(DPA)$_4$-Per**, thus, removing four electrons successively from the system is possible (Fig. 9 and Table 4).

TD-DFT calculations show that the nature of both $S_1 \leftarrow S_0$ transition in **(DPA)$_4$-Per** and **(Bmes$_2$)$_4$-Per** remain HOMO $\rightarrow$ LUMO in character as in perylene. Thus, these transitions can best be described for the **(Bmes$_2$)$_4$-Per** derivative as an LE transition with a small CT contribution whereas there is an increased CT contribution for the **(DPA)$_4$-Per** derivative. This is in accordance with the slightly lower oscillator strengths for the **(DPA)$_4$-Per** derivative ($f = 0.367$ for **(Bmes$_2$)$_4$-Per**; and $f = 0.318$ for **(DPA)$_4$-Per**) and lower extinction coefficients (ε = 20 000 M^{-1} cm^{-1} for **(Bmes$_2$)$_4$-Per** and $\varepsilon = 15\,000$ M^{-1} cm^{-1} for **(DPA)$_4$-Per**). However, the red shift of both λ_{max}(abs) and λ_{max}(em) as well as the larger apparent Stokes shift, agrees well with increasing CT admixture for the **(DPA)$_4$-Per** compound as does the observed solvatochromism, which also results from the CT nature of the lowest excited singlet state, which is not observed for **(Bmes$_2$)$_4$-Per**.

Conclusion

We have synthesized novel *ortho*-tetrasubstituted perylenes with a strong DPA donor or a strong $Bmes_2$ acceptor, which represent the first examples of perylenes substituted only at the *ortho* positions with donors or acceptors. The synthesis of these two systems required two new intermediates **(Br)$_4$-Per** and **(BF$_3$K)-Per**, which could potentially be used for the synthesis of many new *ortho*-perylene derivatives. The donor and the acceptor substituents significantly influence the frontier orbitals which leads to interesting and potentially useful properties. Cyclic voltammetry and square wave voltammetry experiments reveal up to four reversible reductions for the acceptor derivative **(Bmes$_2$)$_4$-Per** and four reversible oxidations for the donor derivative **(DPA)$_4$-Per**, which is unprecedented for perylenes and has only been observed previously for bi(PDI)s. Spectroelectrochemical measurements suggest a strong electronic coupling between the amine moieties through the perylene bridge, which can be categorized as a typical Robin-Day-class-III system. **(DPA)$_4$-Per** reached an unparalleled bathochromic shift of its $S_1 \leftarrow S_0$ transition (λ_{max}(abs) = 499 nm) and emission (λ_{max}(em) = 593 nm) for *ortho*-substituted perylenes which do not have carboxyimide moieties at the *peri*-positions. Both derivatives have unusually long intrinsic singlet lifetimes with that of **(DPA)$_4$-Per** being 94 ns. Transient absorption measurements reveal an additional excited state with a 500 μs lifetime which effectively sensitizes singlet oxygen. This presumed triplet state could prove useful in organo-photocatalysis.[136,140–143] Theoretical studies show that the acceptor $Bmes_2$ couples well with the unoccupied orbitals, which leads to a strong stabilization of the LUMO to LUMO+4 orbitals. However, while the nature of the S_1 state is maintained, the HOMO $\rightarrow$ LUMO transition is less allowed in comparison to the one in perylene. Hence, the radiative decay rates decrease resulting in a longer-lived singlet excited state. The donor DPA also mixes very well with the occupied orbitals, strongly destabilizing the HOMO to HOMO−4 levels. In contrast to the former derivative, its CT character gives rise to a less allowed $S_1 \leftarrow S_0$ transition which results in the slowest radiative decay reported so far for perylenes. Furthermore, it possesses the strongest bathochromic shift observed for *ortho*-perylenes and a large apparent Stokes shift.

Our synthetic procedure has the potential to produce a wide variety of *ortho*-perylene derivatives with a broad range of properties as required for diverse applications. As one can anticipate that alternative donors and acceptors could result in typical π-stacking interactions, which are inhibited in our current compounds, the synthesis of such species is under investigation in our laboratory.

Experimental section

General considerations

The catalyst $[Ir(OMe)(COD)]_2$ [186] and $Pd_2(dba)_3 \cdot CHCl_3$[187] were prepared according to literature procedures. All other starting materials were purchased from commercial sources and used as received. Solvents used for the synthesis were HPLC grade, further treated to remove trace water using a commercial solvent purification system and deoxygenated using the freeze–pump–thaw method. Microwave-heating (95 °C) was performed in a Biotage® initiator + reactor. The reactions were set up in standard 20 mL microwave tubes, which were sealed with crimp caps.

The ^{1}H, ^{13}C{^{1}H}, ^{11}B{^{1}H}, ^{19}F, ^{15}N HMBC NMR spectra were recorded in $CDCl_3$, CD_2Cl_2, or DMSO-d_6 solutions either on a Bruker Avance I HD 500 (^{1}H, 500 MHz; ^{13}C, 125 MHz; ^{11}B, 160 MHz, ^{19}F, 470 MHz) or Bruker Avance III HD 300 (^{1}H, 300 MHz; ^{13}C, 75 MHz; ^{11}B, 96 MHz) spectrometer. ^{1}H NMR and ^{13}C spectra are referenced to the residual protiated solvent $CHCl_3$ (^{1}H, $\delta = 7.26$, $CDCl_3$), CD_2Cl_2 (^{1}H, $\delta = 5.32$, CD_2Cl_2) and DMSO-d_5 (^{1}H, $\delta = 2.50$, DMSO-d_6). ^{13}C NMR spectra were broad-band proton decoupled ^{13}C{^{1}H}. ^{11}B{^{1}H} NMR signals were referenced to external $BF_3 \cdot OEt_2$ and ^{15}N HMBC signals were referenced to $MeNO_2$ + 10% $CDCl_3$. Chemical shifts are listed in parts per million (ppm) and coupling constants in Hertz (Hz). The solid-state magic-angle spinning (MAS) NMR spectra were recorded using a Bruker DSX-400 spectrometer operating at 128 MHz for ^{11}B and 100 MHz for ^{13}C with a 4 mm rotor (o. d.). Chemical shifts were calibrated externally using adamantane (38.48 ppm). Isotropic chemical shifts were estimated by simulating the observed spectrum using the Solid Line Shape Analysis 2.2.4 (SOLA) module in Bruker TopSpin 3.5. The second order quadrupolar powder patterns were simulated to extract the isotropic chemical shifts (δ_{iso}), the quadrupolar constants (C_q) and the asymmetry parameters (η_{Quad}).

HRMS were recorded using a Thermo Scientific Exactive Plus Orbitrap MS system with either an Atmospheric Sample Analysis Probe (ASAP) or by Electrospray Ionization (ESI). Elemental analyses were performed on an Elementar vario MICRO cube elemental analyzer.

Cyclic voltammetry experiments were performed using a Gamry Instruments Reference 600 potentiostat. A standard three-electrode

cell configuration was employed using a platinum disk working electrode, a platinum wire counter electrode, and a silver wire, separated by a *Vycor* tip, serving as the reference electrode. Formal redox potentials are referenced to the ferrocene/ferrocenium ($[Cp_2Fe]^{+/0}$) redox couple by using decamethylferrocene ($[Cp_2^*Fe]$; $E_{1/2} = -0.427$ V in THF and $E_{1/2} = -0.532$ V in CH_2Cl_2) as an internal standard. Tetra-*n*-butylammonium hexafluorophosphate ($[n\text{-}Bu_4N][PF_6]$) or $[n\text{-}Bu_4N][Al(OC(CF_3)_3)_4]$ were employed as supporting electrolytes. Compensation for resistive losses (*iR* drop) was employed for all measurements.

A crystal suitable for single-crystal X-ray diffraction was selected, coated in perfluoropolyether oil, and mounted on a MiTeGen sample holder. Diffraction data were collected on a Bruker X8 Apex II 4-circle diffractometer with a CCD area detector using Mo-Kα radiation generated by a Nonius FR591 rotating anode and monochromated by graphite. The crystal was cooled using an Oxford Cryostream low-temperature device. Data were collected at 100 K. The images were processed and corrected for Lorentz-polarization effects and absorption as implemented in the Bruker software packages. The structure was solved using the intrinsic phasing method (SHELXT)[188] and Fourier expansion technique. All non-hydrogen atoms were refined in anisotropic approximation, with hydrogen atoms 'riding' in idealized positions, by full-matrix least squares against F^2 of all data, using SHELXL[189] software. Diamond[190] software was used for graphical representation. Hirshfeld surfaces were calculated and analyzed using the CrystalExplorer[191] program. Other structural information was extracted using Mercury[192] and OLEX2 [193] software. Crystal data and experimental details are listed in Table S1;† full structural information has been deposited with Cambridge Structural Database. CCDC-1881912.

General photophysical measurements

All photophysical measurements were carried out under an argon atmosphere. All solution state measurements were performed in standard quartz cuvettes (1 cm × 1 cm cross section). UV/Vis absorption spectra were recorded using an Agilent 1100 diode array UV/Vis spectrophotometer. Excitation, emission, lifetime and quantum yield measurements were recorded using an Edinburgh Instruments FLSP920 spectrometer equipped with a 450 W Xenon arc lamp, double monochromators for the excitation and emission pathways, and a red-sensitive photomultiplier (PMT-R928P) and a near-IR PMT as detectors. The measurements were made in right-angle geometry mode and all spectra were fully corrected for the spectral response of the instrument. All solutions used in photophysical measurements had a concentration lower than 10^{-5} M.

Fluorescence quantum yield measurements

Fluorescence quantum yields of the samples were measured using a calibrated integrating sphere (150 mm inner diameter) from Edinburgh Instruments combined with the FLSP920 spectrometer described above. For solution-state measurements, the longest wavelength absorption maximum of the compound in the respective solvent was chosen for the excitation. In order to avoid self-absorption, the emission spectra were measured with dilute samples (*ca.* 0.1 OD at the excitation wavelength).

Fluorescence lifetime measurements

Lifetime measurements were conducted using the time-correlated single-photon counting method (TCSPC) on the FLSP920 spectrometer equipped with a high-speed photomultiplier tube positioned after a single emission monochromator. Measurements were made in right-angle geometry mode, and the emission was collected through a polarizer set to the magic angle. Solutions were excited with either a 315 (pulse width 932.5 ps), 376 (pulse width 72.6 ps) or a 472 nm (pulse width 90.6 ps) pulsed diode laser at repetition rates of 1–5 MHz and were recorded at emission maxima. Decays were recorded to 10 000 counts in the peak channel with a record length of at least 1000 channels. The band-pass of the monochromator was adjusted to give a signal count rate of <20 KHz. Iterative reconvolution of the IRF with one decay function and nonlinear least-squares analysis were used to analyze the data. The quality of all decay fits was judged to be satisfactory, based on the calculated values of the reduced χ^2 and Durbin–Watson parameters and visual inspection of the weighted and autocorrelated residuals.

Transient absorption measurements

Transient absorption spectra were measured with an Edinburgh LP920 laser flash spectrometer equipped with a EKSPLA NT340 Nd : YAG laser with integrated optical parametric oscillator, a 450 W Xe flash lamp, a Hamamatsu R955 photomultiplier and a Tektronix TD3012B oscilloscope for detection of the spectra. The transient maps were obtained by measuring decay profiles in 4 nm steps between *ca.* 25 000 cm^{-1} (400 nm) and 14 085 cm^{-1} (710 nm). The instrument response (*ca.* 8 ns) of the set-up was determined by measuring the scattered light using a LUDOX AS-30 colloidal silica suspension in water. Decay curves were fitted with the tailfit function of the spectrometer software. The quality of all decay fits was judged to be satisfactory, based on the calculated values of the reduced χ^2 and Durbin–Watson parameters and visual inspection of the weighted and autocorrelated residuals. All solvents were spectroscopic grade and were used without further purification. The sample solutions in the quartz cuvettes were carefully degassed by bubbling argon through the solutions. The samples were excited with *ca.* 3–6 ns laser pulses at 10 Hz repetition rate. Measurements were performed at pulse energies of 1.2 mJ (excitation at 460 and 550 nm). The stability of the samples was verified by recording the steady-state absorption spectra before and after the time-resolved measurements.

Spectroelectrochemical measurements

Spectroelectrochemical experiments in reflection mode were performed using an Agilent Cary 5000 spectrometer in combination with a designed sample compartment consisting of a cylindrical PTFE cell with an Infrasil® wedge window with an angle of 0.5° and an adjustable three-in-one electrode (6 mm

platinum disc working electrode, 1 mm platinum counter electrode and pseudo reference electrode). The potentials were adjusted with a Gamry 600 potentiostat and all experiments were measured at room temperature under an argon atmosphere.

Theoretical studies

All calculations (DFT and TD-DFT) were carried out with the program package Gaussian 09 (Rev. E.01)[194] and were performed on a parallel cluster system. GaussView 5.0.9 was used to visualize the results, to measure calculated structural parameters, and to plot orbital surfaces (isovalue: $\pm 0.02[ea_0^{-3}]^{1/2}$). The ground-state geometries were optimized using the B3LYP functional[195–197] in combination with the 6-31G(d) basis set.[198,199] The optimized geometries were confirmed to be local minima by performing frequency calculations and obtaining only positive (real) frequencies. Based on these optimized structures, the lowest-energy gas-phase vertical transitions were calculated (singlets, 10 states) by TD-DFT, using the Coulomb-attenuated functional CAM-B3LYP[200] in combination with the 6-31G+(d,p) basis set. The calculations of the radical mono-cation of **(DPA)$_4$-Per** were done at the density functional level, using UBLYP with 35% exact-exchange admixture, the SVP basis set and a polarizable continuum model accounting for solvent effects. The time dependent (TD-DFT) calculations were done at the same level of theory.[201,202]

(Bpin)$_4$-Per (1)

In an argon-filled glovebox, perylene (1.00 g, 3.96 mmol, 1.00 eq.), B_2pin_2 (5.03 g, 19.8 mmol, 5.00 equiv.), $[Ir(COD)(\mu\text{-}OMe)]_2$ (78.8 mg, 119 μmol, 3.00 mol%), 4,4′-di-*tert*-butyl-2,2′-bipyridine (dtbpy) (63.8 mg, 238 μmol, 6.00 mol%) and THF (100 mL) were added to a Schlenk flask. The mixture was refluxed at 85 °C in an oil bath for 40 h. After cooling to room temperature, the solvent was removed under reduced pressure. The residue was washed with cyclohexane (2 × 20 mL) and MeOH (2 × 20 mL) to give **1** as a yellow solid (2.69 g, 3.56 mmol, 90%). The spectral data matched those reported previously.[45] ^{1}H NMR (300 MHz, $CDCl_3$, r.t.): δ = 8.63 (s, 4H), 8.25 (s, 4H), 1.43 (s, 48H) ppm; 13C{^{1}H} NMR (75 MHz, $CDCl_3$, r.t.): δ = 137.1, 133.4, 132.1, 130.5, 126.8 (br), 126.2, 84.2, 25.1 ppm; ^{11}B{^{1}H} NMR (96 MHz, $CDCl_3$, r.t.): δ = 34.2 ppm; HRMS (ASAP$^+$): *m*/*z* calc. for $[C_{44}H_{56}B_4O_8 + H]^+$ 757.4420; found: $[M + H]^+$ 757.4422 ($|\Delta|$ = 0.26 ppm); elemental analysis calc. (%) for $C_{44}H_{56}B_4O_8$: C 69.89, H 7.47; found: C 69.69, H 7.35.

(BF$_3$K)$_4$-Per (2)

In a round-bottom flask **(Bpin)$_4$-Per** (**1**) (378 mg, 500 μmol, 1.00 equiv.) was dissolved in THF (30 mL). To this solution KHF_2 (469 mg, 6.00 mmol, 12.0 equiv.) in H_2O (3 mL) was added and the mixture was stirred vigorously at room temperature for 20 h. The solvent was removed under reduced pressure and the residue was washed with hot acetone (2 × 40 mL), hot EtOH (2 × 40 mL) and hot MeOH (40 mL) to give the product of **2** as a green solid (335 mg, 496 μmol, 99%). ^{1}H NMR (500 MHz, DMSO-d_6, r.t.): δ = 8.11 (s, 4H), 7.40 (s, 4H) ppm; ^{13}C{^{1}H} NMR (125 MHz, DMSO-d_6, r.t.): δ = 133.8, 129.0, 128.9, 126.8, 122.2 ppm (one C not observed, likely that attached to B); ^{11}B{^{1}H} NMR (160 MHz, DMSO-d_6, RT): δ = 3.9 ppm; ^{19}F{^{1}H} NMR (470 MHz, DMSO-d_6, r.t.): δ = −138.7 ppm.

(Bmes$_2$)$_4$-Per (3)

Under an argon atmosphere, **(BF$_3$K)-Per** (**2**) (1.00 g, 1.48 mmol) and degassed THF (20 mL) were added to a Schlenk flask. The suspension was treated with MesMgBr (0.9 M in THF, 13.6 mmol, 15.1 mL) and the reaction was stirred at room temperature for 72 h. After addition of water (10 mL), the precipitate was collected by filtration. In an ultrasonic bath, the residue was washed successively with H_2O, THF, hexane, ethyl acetate, MeOH and CH_2Cl_2. After each washing process, the solid was separated from the solvent by centrifugation. The product was obtained as a yellow solid (1.58 g, 1.27 mmol, 86%). ^{1}H NMR (500 MHz, $CDCl_3$, r.t.): δ = 8.11 (s, 4H), 7.87 (s, 4H), 6.79 (s, 16H), 2.35 (s, 24H), 2.00 (s, 48H) ppm; ^{13}C{^{1}H} NMR (125 MHz, $CDCl_3$, r.t.): δ = 141.5, 140.9, 140.0, 138.7, 133.8, 132.7, 130.6, 129.4, 128.4, 23.7, 21.4 ppm (one C not observed, likely that attached to B); ^{11}B{^{1}H} SSNMR (128 MHz, r.t.): δ = 72.7 ppm; HRMS (APCI$^+$): *m*/*z* calc. for $[C_{92}H_{96}B_4 + H]^+$ 1245.7957; found: $[M + H]^+$ 1245.7983 ($|\Delta|$ = 2.09 ppm); elemental analysis calcd (%) for $C_{92}H_{96}B_4$: C 88.75, H 7.77; found: C 87.80, H 7.92. As is common for related organo-Bmes$_2$ compounds, the carbon analysis of **(Bmes$_2$)$_4$-Per** is 0.95% below the calculated value, while the hydrogen analysis is satisfactory. This has been described previously to the formation of boron carbide.[89,203,204]

(Br)$_4$-Per (4)

Under aerobic conditions, $CuBr_2$ (710 mg, 3.17 mmol, 12.0 equiv.), **(Bpin)$_4$-Per** (**1**) (200 mg, 0.26 mmol, 1.00 equiv.), MeOH (5 mL), THF (5 mL) and H_2O (5 mL) were added to a 20 mL microwave vial. The vial was sealed and heated to 95 °C for 20 h in a microwave reactor. Reaction progress was monitored by HRMS and revealed that the reaction was not finished, hence another portion of $CuBr_2$ (710 mg, 3.17 mmol, 12.0 equiv.) was added and the reaction mixture was heated at 95 °C for another 20 h. The precipitate was collected by centrifugation and washed with H_2O, MeOH, EDTA (0.1 M) and THF. The solubility of **(Br)$_4$-Per** is too low to obtain NMR spectra in solution. However, the solubility was enough to obtain absorption and emission spectra. Hence, this crude product was used (568 mg) without further purification for the following Buchwald–Hartwig amination reaction. A small part was further purified by Kugelrohr sublimation at 250 °C (0.001 mbar) to afford the title compound as an analytically pure red solid. The yield loss during the Kugelrohr sublimation of **(Br)$_4$-Per** was so large that using the crude product for the following reaction gave higher overall yields. ^{13}C{^{1}H} SSNMR (100 MHz, r.t.) δ = 134.8, 129.6, 127.6, 124.3, 118.0; HRMS (ASAP$^+$): *m*/*z* calcd for $[C_{20}H_8Br_4 + H]^+$: 568.7385; found $[M + H]^+$ 568.7363 ($|\Delta|$ = 3.87 ppm); elemental analysis calcd (%) for $C_{20}H_8Br_4$: C 42.30, H 1.42; found: C 42.47, H 1.56.

(DPA)$_4$-Per (5)

Under an argon atmosphere, crude **(Br)$_4$-Per** (**4**) (568 mg, 1.00 mmol), bis(4-methoxyphenyl)amine (1.15 g, 5.00 mmol, 5.00 equiv.), $Pd_2(dba)_3 \cdot CHCl_3$ (20.7 mg, 0.02 mmol, 2.0 mol%), Sphos (16.4 mg, 0.04 mmol, 4.00 mol%), KO^{t}Bu (0.56 g, 5.00 mmol, 5.00 equiv.) and toluene were added to a Young's tube, which was then sealed. The reaction mixture was stirred at 110 °C for 5 d, until reaction monitoring indicated that the reaction was complete. After cooling to room temperature, water was added, and the organic layer was extracted with CH_2Cl_2 (3 × 200 mL). The combined organic extracts were washed with brine and dried over Na_2SO_4. After removing the solvent under reduced pressure, the crude product was purified by flash chromatography (silica, cyclohexane/CH_2Cl_2 first 1 : 4 then gradually increased to 0 : 1). **(DPA)$_4$-Per** was obtained as an orange-red solid (220 mg, 189 μmol, 19% yield over 2 steps starting from **1**). ^{1}H NMR (500 MHz, CD_2Cl_2, r.t.): $\delta = 7.33$ (d, $J =$ 2.1 Hz, 4H), 7.01–6.99 (m, 16H), 6.80–6.77 (m, 16H), 6.63 (d, $J =$ 2.1 Hz, 4H), 3.78 ppm (s, 24H); $^{13}C\{^1H\}$ NMR (125 MHz, CD_2Cl_2, r.t.): $\delta =$ 156.5, 147.7, 140.9, 137.5, 131.6, 127.0, 120.1, 115.1, 115.0, 114.0, 55.8 ppm; ^{15}N NMR (500 MHz, CD_2Cl_2, RT): $\delta =$ −286.3 ppm; HRMS (APCI$^+$): *m*/*z* calcd for $[C_{76}H_{64}N_4O_8 + H]^+$: 1161.4797; found $[M + H]^+$ 1161.4781 ($|\Delta| = 1.38$ ppm).

Conflicts of interest

The authors declare no conflict of interest.

Acknowledgements

We are grateful for generous financial support by the Bavarian State Ministry of Science, Research, and the Arts for the Collaborative Research Network "Solar Technologies go Hybrid", the DFG (GRK 2112) and the University of Würzburg.

References

1 H. Ito, K. Ozaki and K. Itami, *Angew. Chem., Int. Ed.*, 2017, **56**, 11144–11164.
2 J. Wu, W. Pisula and K. Müllen, *Chem. Rev.*, 2007, **107**, 718–747.
3 H. Zollinger, *Color Chemistry: Syntheses, Properties, and Applications of Organic Dyes and Pigments*, Wiley-VCH, Weinheim, 3rd edn, 2003.
4 W. Herbst, G. Wilker and K. Hunger, *Industrial Organic Pigments: Production, Properties, Applications*, Wiley-VCH, Weinheim, 3rd edn, 2004.
5 N. G. Connelly and W. E. Geiger, *Chem. Rev.*, 1996, **96**, 877–910.
6 T. Kaehler, M. Bolte, H.-W. Lerner and M. Wagner, *Angew. Chem., Int. Ed.*, 2019, DOI: 10.1002/anie.201905823.
7 K. Peneva, G. Mihov, F. Nolde, S. Rocha, J.-i. Hotta, K. Braeckmans, J. Hofkens, H. Uji-i, A. Herrmann and K. Müllen, *Angew. Chem., Int. Ed.*, 2008, **47**, 3372–3375.
8 X. Zhang, S. Rehm, M. M. Safont-Sempere and F. Würthner, *Nat. Chem.*, 2009, **1**, 623–629.
9 T. Weil, T. Vosch, J. Hofkens, K. Peneva and K. Müllen, *Angew. Chem., Int. Ed.*, 2010, **49**, 9068–9093.
10 S. Bhosale, A. L. Sisson, P. Talukdar, A. Fürstenberg, N. Banerji, E. Vauthey, G. Bollot, J. Mareda, C. Röger, F. Würthner, N. Sakai and S. Matile, *Science*, 2006, **313**, 84–86.
11 D. Görl, X. Zhang and F. Würthner, *Angew. Chem., Int. Ed.*, 2012, **51**, 6328–6348.
12 C. Li and H. Wonneberger, *Adv. Mater.*, 2012, **24**, 613–636.
13 F. Würthner, *Chem. Commun.*, 2004, **14**, 1564–1579.
14 F. Würthner, C. R. Saha-Möller, B. Fimmel, S. Ogi, P. Leowanawat and D. Schmidt, *Chem. Rev.*, 2016, **116**, 962–1052.
15 H. Langhals, *Helv. Chim. Acta*, 2005, **88**, 1309–1343.
16 L. Chen, C. Li and K. Müllen, *J. Mater. Chem. C*, 2014, **2**, 1938–1956.
17 G. Li, Y. Zhao, J. Li, J. Cao, J. Zhu, X. W. Sun and Q. Zhang, *J. Org. Chem.*, 2015, **80**, 196–203.
18 Z. Chen, U. Baumeister, C. Tschierske and F. Würthner, *Chem.–Eur. J.*, 2007, **13**, 450–465.
19 C. W. Struijk, A. B. Sieval, J. E. J. Dakhorst, M. van Dijk, P. Kimkes, R. B. M. Koehorst, H. Donker, T. J. Schaafsma, S. J. Picken, A. M. van de Craats, J. M. Warman, H. Zuilhof and E. J. R. Sudhölter, *J. Am. Chem. Soc.*, 2000, **122**, 11057–11066.
20 C. D. Dimitrakopoulos and P. R. L. Malenfant, *Adv. Mater.*, 2002, **14**, 99–117.
21 I. B. Berlman, *Handbook of Fluorescence Spectra of Aromatic Molecules*, Academic Press, New York, 2nd edn, 1971.
22 D. M. Donaldson, J. M. Robertson and J. G. White, *Proc. R. Soc. London, Ser. A*, 1953, **220**, 311–321.
23 H. Shiba and G. Hazato, *Bull. Chem. Soc. Jpn.*, 1949, **22**, 92–96.
24 Z. Chen, C. S. Wannere, C. Corminboeuf, R. Puchta and P. v. R. Schleyer, *Chem. Rev.*, 2005, **105**, 3842–3888.
25 A. Ranganathan and G. U. Kulkarni, *Experimental Crystal Structure Determination*, CCDC 215338, 2004.
26 M. Botoshansky, F. H. Herbstein and M. Kapon, *Helv. Chim. Acta*, 2003, **86**, 1113–1128.
27 A. Camerman and J. Trotter, *Proc. R. Soc. London, Ser. A*, 1964, **279**, 129–146.
28 T. M. Krygowski, A. Ciesielski, B. Swirska and P. Leszczynski, *Pol. J. Chem.*, 1994, 2097–2107.
29 F. H. Allen, O. Kennard, D. G. Watson, L. Brammer, G. Orpen and R. Taylor, *J. Chem. Soc., Perkin Trans. 2*, 1987, S1–S19.
30 A. Ranganathan and G. U. Kulkarni, *Proc. - Indian Acad. Sci., Chem. Sci.*, 2003, **115**, 637–647.
31 J. T. Markiewicz and F. Wudl, *ACS Appl. Mater. Interfaces*, 2015, **7**, 28063–28085.
32 J. R. Platt, *J. Chem. Phys.*, 1949, **17**, 484–495.
33 J. Tanaka, *Bull. Chem. Soc. Jpn.*, 1963, **36**, 1237–1249.
34 Y. Tanizaki, T. Yoshinaga and H. Hiratsuka, *Spectrochim. Acta, Part A*, 1978, **34**, 205–210.
35 J. R. Lakowicz, *Principles of Fluorescence Spectroscopy*, Springer, New York, 2010.

36 H. Langhals, J. Karolin and L. B.-Å. Johansson, *Faraday Trans.*, 1998, **94**, 2919–2922.
37 B. S. Jensen and V. D. Parker, *J. Am. Chem. Soc.*, 1975, **97**, 5211–5217.
38 C. E. Crespo-Hernandez, D. M. Close, L. Gorb and J. Leszczynski, *J. Phys. Chem. B*, 2007, **111**, 5386–5395.
39 M. Montalti and S. L. Murov, *Handbook of Photochemistry*, Taylor & Francis, Boca Raton, 3rd edn, 2006.
40 T. C. Werner, J. Chang and D. M. Hercules, *J. Am. Chem. Soc.*, 1970, **92**, 5560–5565.
41 E. S. Pysh and N. C. Yang, *J. Am. Chem. Soc.*, 1963, **85**, 2124–2130.
42 J. Salbeck, H. Kunkely, H. Langhals, R. W. Saalfrank and J. Daub, *Chimia*, 1989, **43**, 6–9.
43 Y. Zagranyarski, L. Chen, D. Jänsch, T. Gessner, C. Li and K. Müllen, *Org. Lett.*, 2014, **16**, 2814–2817.
44 Y. Li, Y. Hong, J. Guo, X. Huang, H. Wei, J. Zhou, T. Qiu, J. Wu and Z. Zeng, *Org. Lett.*, 2017, **19**, 5094–5097.
45 D. N. Coventry, A. S. Batsanov, A. E. Goeta, J. A. K. Howard, T. B. Marder and R. N. Perutz, *Chem. Commun.*, 2005, 2172–2174.
46 I. A. I. Mkhalid, J. H. Barnard, T. B. Marder, J. M. Murphy and J. F. Hartwig, *Chem. Rev.*, 2010, **110**, 890–931.
47 *Boronic acids: Preparation and Applications in Organic Synthesis, Medicine and Materials*, ed. D. Hall, Wiley-VCH, Weinheim, 2nd edn, 2011.
48 A. G. Crawford, Z. Liu, I. A. I. Mkhalid, M.-H. Thibault, N. Schwarz, G. Alcaraz, A. Steffen, J. C. Collings, A. S. Batsanov, J. A. K. Howard and T. B. Marder, *Chem.–Eur. J.*, 2012, **18**, 5022–5035.
49 S. Nakazono, Y. Imazaki, H. Yoo, J. Yang, T. Sasamori, N. Tokitoh, T. Cédric, H. Kageyama, D. Kim, H. Shinokubo and A. Osuka, *Chem.–Eur. J.*, 2009, **15**, 7530–7533.
50 T. Teraoka, S. Hiroto and H. Shinokubo, *Org. Lett.*, 2011, **13**, 2532–2535.
51 S. Ikeda, N. Aratani and A. Osuka, *Chem. Commun.*, 2012, **48**, 4317–4319.
52 L. D. Tran, J. Ma, A. G. Wong-Foy and A. J. Matzger, *Chem.–Eur. J.*, 2016, **22**, 5509–5513.
53 H. Banda, D. Damien, K. Nagarajan, A. Raj, M. Hariharan and M. M. Shaijumon, *Adv. Energy Mater.*, 2017, **7**, 1701316.
54 P. J. Low, M. A. J. Paterson, H. Puschmann, A. E. Goeta, J. A. K. Howard, C. Lambert, J. C. Cherryman, D. R. Tackley, S. Leeming and B. Brown, *Chem.–Eur. J.*, 2004, **10**, 83–91.
55 V. Bulvic, G. Gu, P. E. Burrows, S. R. Forrest and M. E. Thompson, *Nature*, 1996, **380**, 29.
56 N. Tamoto, C. Adachi and K. Nagai, *Chem. Mater.*, 1997, **9**, 1077–1085.
57 E. Bellmann, S. E. Shaheen, S. Thayumanavan, S. Barlow, R. H. Grubbs, S. R. Marder, B. Kippelen and N. Peyghambarian, *Chem. Mater.*, 1998, **10**, 1668–1676.
58 M. C. Harris and S. L. Buchwald, *J. Org. Chem.*, 2000, **65**, 5327–5333.
59 U. Mitschke and P. Bäuerle, *J. Mater. Chem.*, 2000, **10**, 1471–1507.
60 P. M. Borsenberger and D. S. Weiss, *Organic Photoreceptors for Xerography*, Marcel Dekker, New York, 1998.
61 O. Kwon, S. Barlow, S. A. Odom, L. Beverina, N. J. Thompson, E. Zojer, J.-L. Bredas and S. R. Marder, *J. Phys. Chem.*, 2005, **109**, 9346–9352.
62 M. Stolka, J. F. Yanus and D. M. Pai, *J. Phys. Chem.*, 1984, **88**, 4707–4714.
63 P. M. Borsenberger and D. S. Weiss, *Organic Photoreceptors for Imaging Systems*, Dekker, New York, 1993.
64 M. Thelakkat, R. Fink, F. Haubner and H.-W. Schmidt, *Macromol. Symp.*, 1998, **125**, 157–164.
65 M. Thelakkat, *Macromol. Mater. Eng.*, 2002, **287**, 442.
66 C. W. Tang, *Appl. Phys. Lett.*, 1986, **48**, 183–185.
67 C. W. Tang and S. A. VanSlyke, *Appl. Phys. Lett.*, 1987, **51**, 913–915.
68 E. S. Kolb, R. A. Gaudiana and P. G. Mehta, *Macromolecules*, 1996, **29**, 2359–2364.
69 H. Fujikawa, S. Tokito and Y. Taga, *Synth. Met.*, 1997, **91**, 161–162.
70 C. Giebeler, H. Antoniadis, D. D. C. Bradley and Y. Shirota, *Appl. Phys. Lett.*, 1998, **72**, 2448–2450.
71 M. Redecker, D. D. C. Bradley, M. Inbasekaran, W. W. Wu and E. P. Woo, *Adv. Mater.*, 1999, **11**, 241–246.
72 T. Braig, D. C. Müller, M. Groß, K. Meerholz and O. Nuyken, *Macromol. Rapid Commun.*, 2000, **21**, 583–589.
73 W. E. Moerner and S. M. Silence, *Chem. Rev.*, 1994, **94**, 127–155.
74 S. Dapperheld, E. Steckhan, K.-H. G. Brinkhaus and T. Esch, *Chem. Ber.*, 1991, 2557–2567.
75 S. Amthor, B. Noller and C. Lambert, *Chem. Phys.*, 2005, **316**, 141–152.
76 C. Lambert and G. Nöll, *J. Am. Chem. Soc.*, 1999, **121**, 8434–8442.
77 T. Noda and Y. Shirota, *J. Am. Chem. Soc.*, 1998, **120**, 9714–9715.
78 Y. S. M. Kinoshita, *Chem. Lett.*, 2001, **30**, 614–615.
79 C. D. Entwistle and T. B. Marder, *Angew. Chem., Int. Ed.*, 2002, **41**, 2927–2931.
80 C. D. Entwistle and T. B. Marder, *Chem. Mater.*, 2004, **16**, 4574–4585.
81 L. Ji, S. Griesbeck and T. B. Marder, *Chem. Sci.*, 2017, **8**, 846–863.
82 S. Y. A. Wakamiya, *Bull. Chem. Soc. Jpn.*, 2015, **88**, 1357.
83 Y. Ren and F. Jäkle, *Dalton Trans.*, 2016, **45**, 13996–14007.
84 A. W. S. Yamaguchi, *Pure Appl. Chem.*, 2006, **78**, 1413–1424.
85 F. Jäkle, *Coord. Chem. Rev.*, 2006, **250**, 1107–1121.
86 S.-Y. Li, Z.-B. Sun and C.-H. Zhao, *Inorg. Chem.*, 2017, **56**, 8705–8717.
87 F. Jäkle, *Chem. Rev.*, 2010, **110**, 3985–4022.
88 S.-B. Zhao, P. Wucher, Z. M. Hudson, T. M. McCormick, X.-Y. Liu, S. Wang, X.-D. Feng and Z.-H. Lu, *Organometallics*, 2008, **27**, 6446–6456.
89 S. Griesbeck, Z. Zhang, M. Gutmann, T. Lühmann, R. M. Edkins, G. Clermont, A. N. Lazar, M. Haehnel, K. Edkins, A. Eichhorn, M. Blanchard-Desce, L. Meinel and T. B. Marder, *Chem.–Eur. J.*, 2016, **22**, 14701–14706.

90 S. Griesbeck, M. Ferger, C. Czernetzi, C. Wang, R. Bertermann, A. Friedrich, M. Haehnel, D. Sieh, M. Taki, S. Yamaguchi and T. B. Marder, *Chem.–Eur. J.*, 2019, **25**, 7679–7688.
91 S. Griesbeck, E. Michail, C. Wang, H. Ogasawara, S. Lorenzen, L. Gerstner, T. Zang, J. Nitsch, Y. Sato, R. Bertermann, M. Taki, C. Lambert, S. Yamaguchi and T. B. Marder, *Chem. Sci.*, 2019, **41**, 2927.
92 S. Yamaguchi, T. Shirasaka and K. Tamao, *Org. Lett.*, 2000, **2**, 4129–4132.
93 N. Matsumi, K. Naka and Y. Chujo, *J. Am. Chem. Soc.*, 1998, **120**, 5112–5113.
94 N. Matsumi, K. Naka and Y. Chujo, *J. Am. Chem. Soc.*, 1998, **120**, 10776–10777.
95 A. G. Crawford, A. D. Dwyer, Z. Liu, A. Steffen, A. Beeby, L.-O. Pålsson, D. J. Tozer and T. B. Marder, *J. Am. Chem. Soc.*, 2011, **133**, 13349–13362.
96 L. Ji, R. M. Edkins, A. Lorbach, I. Krummenacher, C. Bruckner, A. Eichhorn, H. Braunschweig, B. Engels, P. J. Low and T. B. Marder, *J. Am. Chem. Soc.*, 2015, **137**, 6750–6753.
97 L. Ji, A. Lorbach, R. M. Edkins and T. B. Marder, *J. Org. Chem.*, 2015, **80**, 5658–5665.
98 H. C. Brown and V. H. Dodson, *J. Am. Chem. Soc.*, 1957, **79**, 2302.
99 Z. Zhang, R. M. Edkins, M. Haehnel, M. Wehner, A. Eichhorn, L. Mailänder, M. Meier, J. Brand, F. Brede, K. Müller-Buschbaum, H. Braunschweig and T. B. Marder, *Chem. Sci.*, 2015, **6**, 5922–5927.
100 Z. Zhou, A. Wakamiya, T. Kushida and S. Yamaguchi, *J. Am. Chem. Soc.*, 2012, **134**, 4529–4532.
101 G. A. Molander and R. Figueroa, *Aldrichimica Acta*, 2005, **38**, 49.
102 S. Darses and J.-P. Genet, *Chem. Rev.*, 2008, **108**, 288–325.
103 G. Berionni, B. Maji, P. Knochel and H. Mayr, *Chem. Sci.*, 2012, **3**, 878–882.
104 A. J. J. Lennox, *Organotrifluoroborate Preparation, Coupling and Hydrolysis*, Springer, Heidelberg, 2013.
105 *Organic Reactions*, ed. S. E. Denmark, John Wiley & Sons, Inc, Hoboken, 79th edn, 2013, vol. 79.
106 J. Merz, J. Fink, A. Friedrich, I. Krummenacher, H. H. Al Mamari, S. Lorenzen, M. Haehnel, A. Eichhorn, M. Moos, M. Holzapfel, H. Braunschweig, C. Lambert, A. Steffen, L. Ji and T. B. Marder, *Chem.–Eur. J.*, 2017, **23**, 13164–13180.
107 K. Schickedanz, J. Radtke, M. Bolte, H.-W. Lerner and M. Wagner, *J. Am. Chem. Soc.*, 2017, **139**, 2842–2851.
108 K. Schickedanz, T. Trageser, M. Bolte, H.-W. Lerner and M. Wagner, *Chem. Commun.*, 2015, **51**, 15808–15810.
109 A. D. Ainley and F. Challenger, *J. Chem. Soc.*, 1930, 2171–2180.
110 A. L. S. Thompson, G. W. Kabalka, M. R. Akula and J. W. Huffman, *Synthesis*, 2005, **36**, 547.
111 C. Näther, H. Bock, Z. Havlas and T. Hauck, *Organometallics*, 1998, **17**, 4707–4715.
112 M. Bolte, *Experimental Crystal Structure Determination*, CCDC 1546182, 2017.
113 F. Würthner, *Pure Appl. Chem.*, 2006, **78**, 2341–2349.
114 M. A. Spackman and P. G. Byrom, *Chem. Phys. Lett.*, 1997, **267**, 215–220.
115 J. J. McKinnon, A. S. Mitchell and M. A. Spackman, *Chem.–Eur. J.*, 1998, **4**, 2136–2141.
116 J. J. McKinnon, M. A. Spackman and A. S. Mitchell, *Acta Crystallogr., Sect. B: Struct. Sci.*, 2004, **60**, 627–668.
117 M. A. Spackman and D. Jayatilaka, *CrystEngComm*, 2009, **11**, 19–32.
118 M. A. Spackman and J. J. McKinnon, *CrystEngComm*, 2002, **4**, 378–392.
119 A. Parkin, G. Barr, W. Dong, C. J. Gilmore, D. Jayatilaka, J. J. McKinnon, M. A. Spackman and C. C. Wilson, *CrystEngComm*, 2007, **9**, 648.
120 J. J. McKinnon, D. Jayatilaka and M. A. Spackman, *Chem. Commun.*, 2007, **267**, 3814.
121 L. Weber, V. Werner, M. A. Fox, T. B. Marder, S. Schwedler, A. Brockhinke, H.-G. Stammler and B. Neumann, *Dalton Trans.*, 2009, 1339.
122 C. Huang, S. Barlow and S. R. Marder, *J. Org. Chem.*, 2011, **76**, 2386–2407.
123 We note, that Zeng and co-workers[44] do not list their extinction coefficients. Therefore, we estimated them from their Fig. 1.
124 The Stokes shift is defined as the energy difference between the 0–0 transitions of the absorption and the emission. However, as the first transition is broad, the band maxima of the absorption and emission have been used to determine the Stokes shift throughout the paper. Consequently, the term "apparent Stokes shift" is used.
125 É. Torres, M. N. Berberan-Santos and M. J. Brites, *Dyes Pigm.*, 2015, **112**, 298–304.
126 We note that we also measured the emission of **(Br)$_4$-Per** in CH_2Cl_2 for full comparison with the brominated derivative from Zeng and co-workers as they only give photophysical results in CH_2Cl_2 (see ESI Fig. S1†).
127 M.-J. Lin, Á. J. Jiménez, C. Burschka and F. Würthner, *Chem. Commun.*, 2012, **48**, 12050–12052.
128 F. Schlosser, V. Stepanenko and F. Würthner, *Chem. Commun.*, 2010, **46**, 8350–8352.
129 M. Zander, H. Dreeskamp and E. Koch, *Z. Naturforsch., A: Phys. Sci.*, 1974, **29**, 1518–1519.
130 H. Dreeskamp, E. Koch and M. Zander, *Chem. Phys. Lett.*, 1975, **31**, 251–253.
131 K. Nagarajan, A. R. Mallia, V. S. Reddy and M. Hariharan, *J. Phys. Chem. C*, 2016, **120**, 8443–8450.
132 S. K. M. Nalluri, J. Zhou, T. Cheng, Z. Liu, M. T. Nguyen, T. Chen, H. A. Patel, M. D. Krzyaniak, W. A. Goddard, M. R. Wasielewski and J. F. Stoddart, *J. Am. Chem. Soc.*, 2019, **141**, 1290–1303.
133 S. J. Strickler and R. A. Berg, *J. Chem. Phys.*, 1962, **37**, 814–822.
134 H. Dreeskamp, A. Läufer and M. Zander, *Z. Naturforsch., A: Phys. Sci.*, 1983, **38**, 698–700.
135 J. Zhao, W. Wu, J. Sun and S. Guo, *Chem. Soc. Rev.*, 2013, **42**, 5323–5351.
136 H. Xiang, J. Cheng, X. Ma, X. Zhou and J. J. Chruma, *Chem. Soc. Rev.*, 2013, **42**, 6128–6185.

137 A. Gut, Ł. Łapok, D. Drelinkiewicz, T. Pędziński, B. Marciniak and M. Nowakowska, *Chem.–Asian J.*, 2018, **13**, 55–65.
138 Q. Zhao, F. Li and C. Huang, *Chem. Soc. Rev.*, 2010, **39**, 3007–3030.
139 Y. Feng, J. Cheng, L. Zhou, X. Zhou and H. Xiang, *Analyst*, 2012, **137**, 4885–4901.
140 J.-P. Fouassier, F. Morlet-Savary, J. Lalevée, X. Allonas and C. Ley, *Materials*, 2010, **3**, 5130–5142.
141 M. L. Marin, L. Santos-Juanes, A. Arques, A. M. Amat and M. A. Miranda, *Chem. Rev.*, 2012, **112**, 1710–1750.
142 N. Noto, T. Koike and M. Akita, *Chem. Sci.*, 2017, **8**, 6375–6379.
143 N. Noto, Y. Tanaka, T. Koike and M. Akita, *ACS Catal.*, 2018, **8**, 9408–9419.
144 I. Ghosh, T. Ghosh, J. I. Bardagi and B. König, *Science*, 2014, **346**, 725–728.
145 T. N. Singh-Rachford and F. N. Castellano, *Coord. Chem. Rev.*, 2010, **254**, 2560–2573.
146 J. Zhao, S. Ji and H. Guo, *RSC Adv.*, 2011, **1**, 937.
147 M. R. Detty, S. L. Gibson and S. J. Wagner, *J. Med. Chem.*, 2004, **47**, 3897–3915.
148 L. Sobotta, P. Skupin-Mrugalska, J. Mielcarek, T. Goslinski and J. Balzarini, *Mini-Rev. Med. Chem.*, 2015, **15**, 503–521.
149 W. E. Ford and P. V. Kamat, *J. Phys. Chem.*, 1987, **91**, 6373–6380.
150 A. J. Tilley, R. D. Pensack, T. S. Lee, B. Djukic, G. D. Scholes and D. S. Seferos, *J. Phys. Chem. C*, 2014, **118**, 9996–10004.
151 M. T. Vagnini, A. L. Smeigh, J. D. Blakemore, S. W. Eaton, N. D. Schley, F. D'Souza, R. H. Crabtree, G. W. Brudvig, D. T. Co and M. R. Wasielewski, *Proc. Natl. Acad. Sci. U. S. A.*, 2012, **109**, 15651–15656.
152 M. Schulze, A. Steffen and F. Würthner, *Angew. Chem., Int. Ed.*, 2015, **127**, 1590–1593.
153 A. A. Rachford, S. Goeb and F. N. Castellano, *J. Am. Chem. Soc.*, 2008, **130**, 2766–2767.
154 H. Weissman, E. Shirman, T. Ben-Moshe, R. Cohen, G. Leitus, L. J. W. Shimon and B. Rybtchinski, *Inorg. Chem.*, 2007, **46**, 4790–4792.
155 B. Ventura, H. Langhals, B. Böck and L. Flamigni, *Chem. Commun.*, 2012, **48**, 4226–4228.
156 L. Flamigni, A. Zanelli, H. Langhals and B. Böck, *J. Phys. Chem. A*, 2012, **116**, 1503–1509.
157 E. Oliveros, S. H. Bossmann, S. Nonell, C. Martí, G. Heit, G. Tröscher, A. Neuner, C. Martínez and A. M. Braun, *New J. Chem.*, 1999, **23**, 85–93.
158 C. Schweitzer and R. Schmidt, *Chem. Rev.*, 2003, **103**, 1685–1757.
159 A. A. Abdel-Shafi and F. Wilkinson, *J. Phys. Chem. A*, 2000, **104**, 5747–5757.
160 A. J. McLean, D. J. McGarvey and T. G. Truscott, *J. Chem. Soc., Faraday Trans.*, 1990, **86**, 3075–3080.
161 J. D. Harris, M. J. Moran and I. Aprahamian, *Proc. Natl. Acad. Sci. U. S. A.*, 2018, **115**, 9414–9422.
162 A. B. Buades, V. Sanchez Arderiu, D. Olid-Britos, C. Viñas, R. Sillanpää, M. Haukka, X. Fontrodona, M. Paradinas, C. Ocal and F. Teixidor, *J. Am. Chem. Soc.*, 2018, **140**, 2957–2970.
163 M. Frasconi, I. R. Fernando, Y. Wu, Z. Liu, W.-G. Liu, S. M. Dyar, G. Barin, M. R. Wasielewski, W. A. Goddard and J. F. Stoddart, *J. Am. Chem. Soc.*, 2015, **137**, 11057–11068.
164 J. Kübel, R. Schroot, M. Wächtler, U. S. Schubert, B. Dietzek and M. Jäger, *J. Phys. Chem. C*, 2015, **119**, 4742–4751.
165 Y.-M. Tian, X.-N. Guo, M. W. Kuntze-Fechner, I. Krummenacher, H. Braunschweig, U. Radius, A. Steffen and T. B. Marder, *J. Am. Chem. Soc.*, 2018, **140**, 17612–17623.
166 L. Ramaley and M. S. Krause, *Anal. Chem.*, 1969, 1362–1365.
167 G. C. Barker and I. L. Jenkins, *Analyst*, 1952, **77**, 685–696.
168 I. Raabe, K. Wagner, K. Guttsche, M. Wang, M. Grätzel, G. Santiso-Quiñones and I. Krossing, *Chem.–Eur. J.*, 2009, **15**, 1966–1976.
169 F. Barrière and W. E. Geiger, *J. Am. Chem. Soc.*, 2006, **128**, 3980–3989.
170 Y. Fan, K. Ziabrev, S. Zhang, B. Lin, S. Barlow and S. R. Marder, *ACS Omega*, 2017, **2**, 377–385.
171 W. Jiang, C. Xiao, L. Hao, Z. Wang, H. Ceymann, C. Lambert, S. Di Motta and F. Negri, *Chem.–Eur. J.*, 2012, **18**, 6764–6775.
172 W. Jiang, L. Ye, X. Li, C. Xiao, F. Tan, W. Zhao, J. Hou and Z. Wang, *Chem. Commun.*, 2014, **50**, 1024–1026.
173 H. Horinouchi, H. Sakai, Y. Araki, T. Sakanoue, T. Takenobu, T. Wada, N. V. Tkachenko and T. Hasobe, *Chem.–Eur. J.*, 2016, **22**, 9631–9641.
174 L. Echegoyen and L. E. Echegoyen, *Acc. Chem. Res.*, 1998, **31**, 593–601.
175 M. Takase, V. Enkelmann, D. Sebastiani, M. Baumgarten and K. Müllen, *Angew. Chem., Int. Ed.*, 2007, **46**, 5524–5527.
176 K. Oki, M. Takase, S. Mori, A. Shiotari, Y. Sugimoto, K. Ohara, T. Okujima and H. Uno, *J. Am. Chem. Soc.*, 2018, **140**, 10430–10434.
177 Y. Shibano, T. Umeyama, Y. Matano, N. V. Tkachenko, H. Lemmetyinen and H. Imahori, *Org. Lett.*, 2006, **8**, 4425–4428.
178 B. Badger and B. Brocklehurst, *Trans. Faraday Soc.*, 1970, **66**, 2939–2947.
179 We note that it is a semantic issue as to whether small delocalized systems are called "MV" compound as it is arbitrary or even impossible to identify redox centers. In fact, the term "charge-resonance" compound is often used.[178] However, in this paper we use the term "mixed valence" compounds.
180 A. Heckmann and C. Lambert, *Angew. Chem., Int. Ed.*, 2012, **51**, 326–392.
181 B. S. Brunschwig and N. Sutin, *Coord. Chem. Rev.*, 1999, **187**, 233–254.
182 B. S. Brunschwig, C. Creutz and N. Sutin, *Chem. Soc. Rev.*, 2002, **31**, 168–184.
183 R. J. Cave and M. D. Newton, *Chem. Phys. Lett.*, 1996, **249**, 15–19.
184 R. J. Cave and M. D. Newton, *J. Chem. Phys.*, 1997, **106**, 9213.

185 M. J. G. Peach, P. Benfield, T. Helgaker and D. J. Tozer, *J. Chem. Phys.*, 2008, **128**, 44118.
186 R. Uson, L. A. Oro, J. A. Cabeza, H. E. Bryndza and M. P. Stepro, in *Inorganic Syntheses*, ed. Kirschner (Hg.), 1985, pp. 126–130.
187 S. S. Zalesskiy and V. P. Ananikov, *Organometallics*, 2012, **31**, 2302–2309.
188 G. M. Sheldrick, *Acta Crystallogr., Sect. A: Found. Adv.*, 2015, **71**, 3–8.
189 G. M. Sheldrick, *Acta Crystallogr., Sect. A: Found. Crystallogr.*, 2008, **64**, 112–122.
190 K. B. H. Putz, *Diamond, Crystal and Molecular Structure Visualization, Crystal Impact*, H. Putz & K., Brandenburg GbR, Bonn (Germany), 2017.
191 M. J. Turner, J. J. McKinnon, S. K. Wolff, D. J. Grimwood, P. R. Spackman, D. Jayatilaka and M. A. Spackman, *CrystalExplorer17*, University of Western Australia, 2017.
192 C. F. Macrae, I. J. Bruno, J. A. Chisholm, P. R. Edgington, P. McCabe, E. Pidcock, L. Rodriguez-Monge, R. Taylor, J. van de Streek and P. A. Wood, *J. Appl. Crystallogr.*, 2008, **41**, 466–470.
193 O. V. Dolomanov, L. J. Bourhis, R. J. Gildea, J. A. K. Howard and H. Puschmann, *J. Appl. Crystallogr.*, 2009, **42**, 339–341.
194 M. J. Frisch, G. W. Trucks, H. B. Schlegel, G. E. Scuseria, M. A. Robb, J. R. Cheeseman, G. Scalmani, V. Barone, B. Mennucci, G. A. Petersson, H. Nakatsuji, M. Caricato, X. Li, H. P. Hratchian, A. F. Izmaylov, J. Bloino, G. Zheng, J. L. Sonnenberg, M. Hada, M. Ehara, K. Toyota, R. Fukuda, J. Hasegawa, M. Ishida, T. Nakajima, Y. Honda, O. Kitao, H. Nakai, T. Vreven, J. A. Montgomery Jr, J. E. Peralta, F. Ogliaro, M. Bearpark, J. J. Heyd, E. Brothers, K. N. Kudin, V. N. Staroverov, R. Kobayashi, J. Normand, K. Raghavachari, A. Rendell, J. C. Burant, S. S. Iyengar, J. Tomasi, M. Cossi, N. Rega, J. M. Millam, M. Klene, J. E. Knox, J. B. Cross, V. Bakken, C. Adamo, J. Jaramillo, R. Gomperts, R. E. Stratmann, O. Yazyev, A. J. Austin, R. Cammi, C. Pomelli, J. W. Ochterski, R. L. Martin, K. Morokuma, V. G. Zakrzewski, G. A. Voth, P. Salvador, J. J. Dannenberg, S. Dapprich, A. D. Daniels, Ö. Farkas, J. B. Foresman, J. V. Ortiz, J. Cioslowski and D. J. Fox, *Gaussian 09, Revision E.01*, Gaussian, Inc., Wallingford CT, 2009.
195 A. D. Becke, *J. Chem. Phys.*, 1993, **98**, 5648.
196 C. Lee, W. Yang and R. G. Parr, *Phys. Rev. B: Condens. Matter Mater. Phys.*, 1988, **37**, 785–789.
197 P. J. Stephens, F. J. Devlin, C. F. Chabalowski and M. J. Frisch, *J. Phys. Chem.*, 1994, **98**, 11623–11627.
198 G. A. Petersson and M. A. Al-Laham, *J. Chem. Phys.*, 1991, **94**, 6081.
199 G. A. Petersson, A. Bennett, T. G. Tensfeldt, M. A. Al-Laham and W. A. Shirley, *J. Chem. Phys.*, 1988, 2193–2218.
200 T. Yanai, D. P. Tew and N. C. Handy, *Chem. Phys. Lett.*, 2004, **393**, 51–57.
201 M. Renz, K. Theilacker, C. Lambert and M. Kaupp, *J. Am. Chem. Soc.*, 2009, **131**, 16292–16302.
202 M. Kaupp, M. Renz, M. Parthey, M. Stolte, F. Würthner and C. Lambert, *Phys. Chem. Chem. Phys.*, 2011, **13**, 16973–16986.
203 J. C. Collings, S.-Y. Poon, C. Le Droumaguet, M. Charlot, C. Katan, L.-O. Pålsson, A. Beeby, J. A. Mosely, H. M. Kaiser, D. Kaufmann, W.-Y. Wong, M. Blanchard-Desce and T. B. Marder, *Chem.–Eur. J.*, 2009, **15**, 198–208.
204 S.-F. Liu, Q. Wu, H. L. Schmider, H. Aziz, N.-X. Hu, Z. Popović and S. Wang, *J. Am. Chem. Soc.*, 2000, **122**, 3671–3678.